ABSTRACT

VARMA, MANJU R. Vapor Phase Lubrication of MicroElectro Mechanical Systems (MEMS): An atomistic approach to solve friction and stiction in MEMS. (Under the direction of Dr. Jacqueline Krim).

The motivation for this thesis is the desire to overcome the problem associated with reliability and yield of these staggeringly small devices called MicroElectro Mechanical Systems (MEMS). The field of microelctromechanical systems involves the interaction of the physical environment with electrical signals through the use of microbatch-fabricated devices. MEMS is an emerging technology which finds applications in diverse fields such as automotive, medicine, aeronautics, communication and defense. The device dimensions range well into the micrometer regime and are soon approaching the length scales studied by nanotribologists Though the MEMS technology has made a substantial impact over the past decade at the device or component level, it has yet to realize a wide range commercial success. Stiction, adhesion, friction and wear seem to be the main deterrents to their lifetime, and hence full commercialization of these devices. These problems can be attributed to the high surface-to-volume ratio, substantial solid surface nanocontacts, close proximity of microstructures and a myriad other device complications.

Several researchers have come up with solutions to avoid release-related stiction, but in-use stiction and friction still persist, proving detrimental to the life span of these microstructures. Though a variety of engineering solutions have been employed to solve them, lubrication of these microelectromechanical systems still remains to be a difficult issue because, the semiconductor like fabrication and small size makes lubrication a challenge in crevices and surfaces beyond the line of sight. In this study, an attempt is made to investigate the in-use stiction and frictional effects by screening vapor phase lubricants on materials of relevance to MEMS using modern nanotribological techniques. The surface effects of silicon after screening vapor phase lubricants are studied using Quartz Crystal Microbalance (QCM)

technique in ultra high vacuum. The most promising candidates are then screened on specially designed microstructures called Sidewall tribometers or Friction testers, to study the frictional and wear characteristics. The primary advantage of thermally activated vapor phase lubrication approach is conformality and *in-situ* replenishment of the lubricant as the lubricating film is worn away.

We have studied the adsorption of the vapor phase lubricant t-butyl phenyl phosphate (TBPP) on Si and Si-OTS (octadecyltrichlorosilane) surfaces. Results show that this particular vapor phase lubricant and the SAM coating of OTS show a synergistic relationship. TBPP not only lubricates OTS but acts as a protective coat at high temperatures.

We have managed to build a system for the uptake of vapor phase lubricants on the MEMS friction testers under vacuum conditions. This new and improved friction test setup will help in understanding the frictional characteristics of these microstructures, and possibly aid in developing a reliable solution to overcome the myriad problems associated with friction and stiction of MicroElectro Mechanical Systems. The following thesis report describes the status of the project and a summary of results.

VAPOR PHASE LUBRICATION OF MICROELECTRO MECHANICAL SYSTEMS (MEMS): AN ATOMISTIC APPROACH TO SOLVE FRICTION AND STICTION IN MEMS

by

Manju R. Varma

A thesis submitted to the Graduate Faculty of
North Carolina State University
In partial fulfillment of the requirements for the
M.S Degree

Department of Electrical and Computer Engineering

Raleigh, 2003

Approved by:

Dr. Jacqueline Krim Chair of the Advisory Committee	Dr. Veena Misra
Dr. Griff Bilbro	Dr. Christine Grant

To my parents, Rathna Varma and Shailaja,

for all their love and support,

for raising me with the freedom to make my own choices.

BIOGRAPHY

Manju Varma was born on August 17th, 1978, in Mysore, India. In 1996, she started her undergraduate work at Sri Jayachamarajendra College of Engineering affiliated to University of Mysore, India. After 4 years of college, which included research experience at Indian Institute of Science (IISc), Bangalore, she graduated with a Bachelor of Science degree in Electronics and Communication Engineering. She worked for nine months at ***i-flex Solutions*** ltd., Bangalore, as an Associate Consultant before leaving to the United States to pursue her Masters.

In fall 2001, she joined the Masters program in the department of Electrical and Computer Engineering at North Carolina State University, Raleigh, NC. While working towards her masters degree, she was a research assistant in the Physics department, and was part of the MEMS project. She is a member of the Institute of Electrical and Electronic Engineers.

With the defense of this thesis, she is receiving Master of Science degree in Electrical Engineering from North Carolina State University.

ACKNOWLEDGEMENTS

I wish to express my sincere gratitude to my thesis advisor, Dr. Jacqueline Krim for her invaluable support and guidance throughout my stay at NC State University. She has always been available to discuss technical and non-technical issues related to my thesis and has helped me overcome all the difficulties that I encountered. I thank Dr. Veena Misra, Dr. Griff Bilbro and Dr. Christine Grant for being members of my thesis committee. They have been very interested in my work and eager to learn developments in this field.

I'm greatly indebted to *Papa* and *Mamma* for everything that they've done to me in my life. Without their love and affection, I would not have been able to succeed in my endeavors in this country, away from home. I wish to thank Chetan for all the love and support, during these difficult times. He has backed me in all the decisions that I've made.

I wish to thank Worakarn, popularly known as B, for working with me through all those late-evening and night hours and for helping me set-up all the experimental equipment. I also thank my other group members – Cherno, Mohammed, Sang Min, Steve, Tonya, Matt and Adam – for helping me clear my doubts in Physics and for their comments about my thesis. Special thanks to my friend Guru for all the enlightening discussions I've had with him throughout various stages of my thesis. His sympathetic ear deserves special mention.

Finally, I would like to thank all my friends here at NC State, who made this a fun-filled and worthwhile stay.

TABLE OF CONTENTS

LIST OF FIGURES

CHAPTER 1

INTRODUCTION

1.1 MEMS and their applications

MicroElectro Mechanical Systems or MEMS form a group of micro devices that are in fact beginning to affect many areas of science and technology. This field deals with the interaction of physical or mechanical elements with electrical signals through the use of micro devices. The miniature size being the most important feature of these devices, they are typically no bigger than a grain of sand. They virtually act as the interface between the electronics and the physical world, allowing the integration of electronics and mechanical elements on a single chip. This emerging technology finds applications in diverse fields like automotive, medicine, aeronautics, communication and defense.

Pressure sensors, accelerometers, actuators and optical switches have been deployed in large numbers for commercial applications. The small size, low power consumption, high switching density and low-cost batch processing of these devices makes them perfect for optical switching applications. Radio frequency MicroElectro Mechanical Systems or rfMEMS is another growing area in commercial MEMS technology. They are becoming an archetype in cell phones and other wireless technology products. Medical MEMS are used in vivo implants and surgical

procedures, which are performed in confined spaces. Their small size helps in analyzing living cells at the microscopic scale.

The automotive industry was one of the first to embrace MEMS commercially through crash airbag accelerometers. These accelerometers due to their high sensitivity provide quick response to deceleration. Compactness and high sensitivity have made them a favorite product in automotive airbags. Further improvements are being made wherein the response of the airbags are calculated according to the size and weight of the person seated in the automobile.

Realization of commercial products using MEMS, shows that work in this area has moved past the research stage, with multitudinous applications already established and many more arriving. Richard Feyman, in his talk titled 'There's plenty of room in the bottom' at the American Physical Society in 1959 predicted the development of these micro-devices and addressed issues like inertial and frictional forces, electrostatic actuation and techniques of fabrication which form the basic elements for the anabasis of these miniature devices.

MEMS technology can be classified in general into microscale devices, which follow the batch processing techniques of the IC (Integrated Circuit) industry and mesoscale devices, which are produced using materials like plastic, ceramics, metals and are of the order of millimeters in size. The first category of MEMS devices, the silicon microstructures are produced by following similar procedures as in silicon Integrated Circuits. Materials like polysilicon, silicon dioxide, silicon nitride and gold are stacked and patterned in sequence to produce the required structure. At the final stage of fabrication, the device is released by etching away the sacrificial silicon dioxide and the material around it, leaving some sections free to move. Since these microstructures can be manufactured in parallel and in bulk, they are fairly inexpensive although complicated.

1.1.2 Micromachining

Micromachining is a term given to the process of fabricating the MEMS devices. Commonly used micromachining processes are (1) Surface micromachining

and (2) Bulk micromachining.

Surface micromachining process follows the CMOS (Complementery Metal-Oxide-Semiconductor) technology used for the fabrication of VLSI (Very Large Scale Integration) chips. It is an additive process, which involves deposition, photolithographic patterning and selective etching of multi-layered thin films to form the desired structure. The most important feature being the use of sacrificial oxide layer which is first deposited to act as a platform and later etched to release the free-standing device which is accomplished by either dry/wet etching processes that are relatively insensitive to the microstructure. Typically, the polycrystalline silicon forms the structural material, silicon dioxide the sacrificial material and silicon nitride forms the electrical isolation layer [3].

Figure 1.1 gives a schematic illustration of the surface micromachining process.

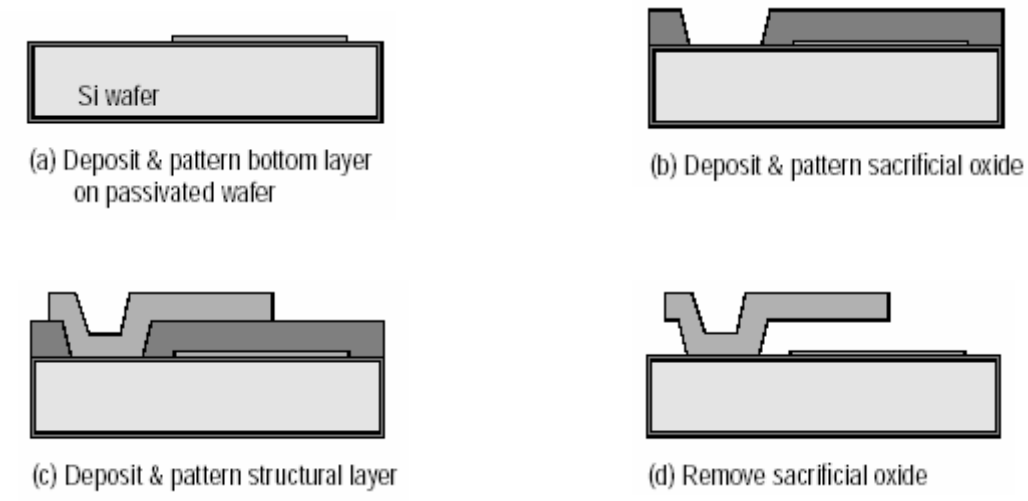

Figure 1.1

Bulk micromachining on the other hand involves etching into the substrate to form complicated microstructures. These etch techniques may be compatible with the CMOS processing. Bulk etchants may be isotropic, that etch different crystallographic directions at different rates (e.g HNA) or anisotropic, that etch all directions in the silicon wafer at the same rate (e.g KOH, NaOH etc), and the phase of the reactants may be liquid, vapor or plasma. Etching reactions rely on the

oxidation of silicon to form compounds, which can be physically purged from the substrate. Structures fabricated from bulk micromachining process include holes, membranes, pits etc.

Figure 1.2 illustrates the bulk micromachining process.

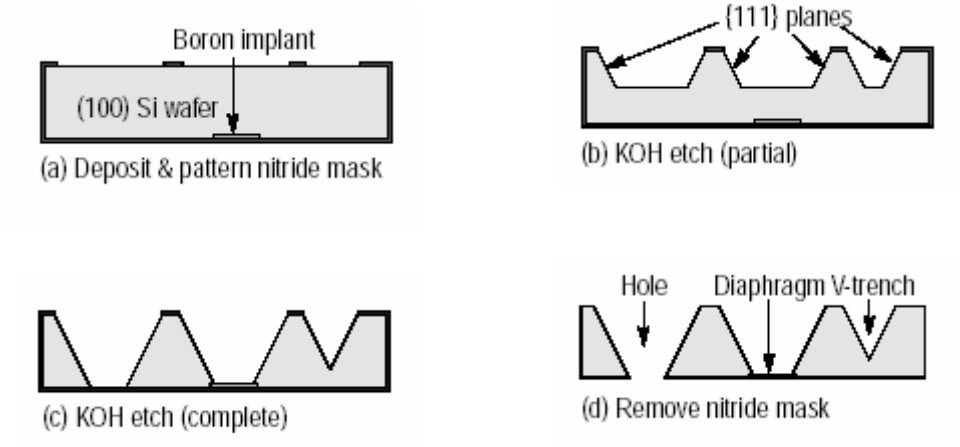

Figure 1.2

Wet etching involves the use of highly reactive species (acids and bases) which oxidize the silicon to form compounds that are soluble in the etching solution. Vapor phase etching is done using reactive gases or vapors. It includes fluorine-containing compounds and laser-driven processes. Some vapor phase etchants include Xenon Diflouride and Interhalogen etchants. Plasma or the RIE (Reactive Ion Etching) is the predominant etch used in surface micromachining today. RF energy is used to drive chemical reactions through the formation of plasma. Etching of the wafer occurs from chemical and physical mechanisms.

1.2 Objective of present study

As mechanical elements shrink in size, the relative importance of surface forces, among all physical effects, become predominant. MicroElectro Mechanical Systems, where the device components have staggeringly small dimensions are soon approaching the length scales studied by nanotribologists. High surface-to-volume ratio, substantial solid surface nanocontacts, close proximity of microstructures, and

innumerable other device complications are associated with their stiction, adhesion, friction and wear characteristics.

The inherent mechanical nature of these devices brings about these myriad complicated problems which are severely limiting their yield and lifetimes. The mass production of MicroElecto Mechanical Systems is comparable with that of Integrated circuits, but only to the stage of the release of these microstructures. Release brings about problems like strong adhesion and stiction, which can permanently damage the microstructure. Post-release problems include friction, wear and tear owing to the topology and the mechanics of the contacting asperities. Reliability is a major impediment for the full commercialization of these devices.

1.2.1 Stiction and Friction

Stiction remains to be a crucial problem in the reliability and lifespan of these devices. The word stiction refers to unintentional adhesion of freestanding structures to the substrate or to neighboring microstructures in close proximity. This occurs when the restoring forces are unable to overcome the interfacial forces like capillary forces, van der waals forces, electrostatic forces etc.

Release related stiction occurs during the final rinsing stages of the sacrificial oxide layer etch. Typically the etchant is rinsed and the microstructure dried through evaporation to obtain the free-standing structure. But during the final stage, the possibility of the compliant structure adhering to the substrate owing to the capillary action induced by the droplet in the gap is extreme. This may render the device useless if even after drying, the adhesive forces between the contacted areas are more than the restoring forces. Revising the surface to reduce the contact area [4], changing the water minuscus shape [5], supercritical drying [6], freeze sublimation drying have been one of the many solutions devised to avoid release related stiction. However these techniques do not avoid stiction from occurring during the operation of the device.

Figure 1.3 illustrates release-related stiction owing to the capillary forces.

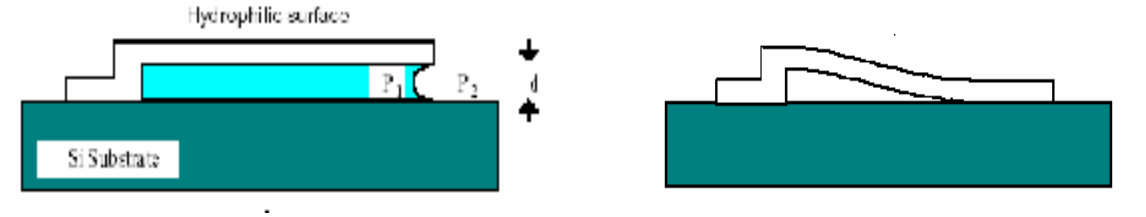

Figure 1.3

In-use stiction comes into picture when microstructure surfaces adhere to one-another due to electrostatic forces or difference in electric potential, a situation common in MEMS devices. When these forces exceed the restoring forces, surfaces tend to adhere permanently leading to the failure of the device. Friction is another uncharacterized property of MicroElectro Mechanical Systems that can significantly impact their performance and reliability. Frictional effects include impact on the dynamical behavior of MEMS and inducing wear that can result in device failure [7].

1.2.2 Lubrication of MicroElectro Mechanical Systems

A variety of engineering solutions have been employed to avoid in-use stiction. They include surface modification techniques involving the deposition of Self-Assembled Monolayers (SAMs)[9], chemical modification of the MEMS surfaces involving hydrogen passivation by ammonium fluoride [10], plasma deposition of Teflon-like fluorocarbon films etc. With SAMs, performance is defenitely improved but in time the coating may wear off which leads to failure. The long-term reliability of the hydrogen passivation method is limited since the hydrogen terminations are metastable and thermally unstable [11].

Lubrication of these micromachined devices still remains an important issue for their robust, reliable and long-term operation. Lubricants are used to reduce friction and wear between two solid sliding surfaces. A lubricant can either be a liquid or a solid, such as graphite and molybdenum disulfide. Selection of a lubricant for a micromachine is complicated in ways that are not so abstruse in case of macro-machines. The semiconductor like fabrication and small size makes lubrication extremely difficult in crevices and surfaces beyond the line of sight. Liquid lubricants

can pose problems in terms of capillary action and viscosity. Solid-film lubricants on the other hand are typically of the same size as these MEMS devices and hence do not serve the purpose.

In this study, we have investigated the stiction and frictional effects of screening vapor phase lubricants on materials of relevance to MEMS using modern nanotribological techniques. These lubricants are also tested on the Sidewall Tribometer devices, also called the Friction Testers supplied by Sandia National Labs.

1.2.3 Vapor Phase Lubrication (VPL)

Lubricating with a vapor is fundamentally and radically very different from other methods of lubrication. Vapor Phase lubrication is a technique wherein chemical reactions are used to form a solid lubricating film on the bearing surfaces even as the lubricating film is being worn away. This technique has an advantage over other lubrication methods especially in high temperature contacts.

Most of the solid lubricating films on the surface is formed by the reaction between the gas and the surface material. This may or may not consume the surface material in the formation of the lubricious film. Some examples include decomposition of TCP (Tricresylphosphate) when exposed to iron surfaces to form an anti-wear, anti-corrosive lubricating film. Also, the reaction between boric oxide and water vapor has shown to form a lubricious film in the form of boric acid at room temperatures.

Decomposition of these solid lubricating films may occur by a reaction process on the surface material rather than with the surface material. This may be the case with hydrocarbons. This decomposition process which is thermally activated can provide low-friction co-efficient and hence good surface protection. Commercially, vapor phase lubricants are used for the lubrication of jet engines, heavy-duty vehicles and metal processing industries.

The most important feature of vapor phase lubricants is the *in-situ* replenishment of the lubricant on the surface as the lubricating film is worn away. This certainly turns out to be an ideal property to lubricate both macroscopic and microscopic surfaces. Being supplied in the vapor phase, the lubricant will find it's way and deposit itself much more easily in crevices and surfaces beyond the line of sight in these micromachined devices and hence forms an ideal candidate for their lubrication. In particular, we study the surface effects of silicon after screening vapor phase lubricants using modern nanotribological techniques.

1.2.4 Ultra High Vacuum (UHV)

Ultra High Vacuum is a technique used in most of the surface science studies, which includes efforts to identify and isolate certain characteristics of surfaces which would affect their tribological properties.

Ultra High Vacuum would enable atomically clean surfaces to be studied without undue interference from contaminants and oxidation. It is also possible to study in cases such as Vapor Phase Lubrication, the complex reactions that occur at the gas-surface interface to form the lubricating solid film. Studies such as these are possible because of the extreme low-pressure level of about 10^-10 torr. At such low pressures, the time taken for any contamination to build up is much greater than the time taken to conduct an experiment, in other words hours are needed before the sample is degraded. The goal here, of course, is to obtain results of sufficiently high quality under better known conditions that will allow the study of frictional and stiction effects of vapor phase lubricants on MEMS devices.

CHAPTER 2

RELATED WORK

2.1 Introduction

In this chapter, I will briefly summarize the related work that has been previously published on this thesis topic.

2.1.1 Organization of the chapter

An important aspect of this thesis is the exploration of how to overcome failures of micro-machines due to in-use stiction and friction. Section 2.2 briefly outlines the various approaches devised to solve release-related stiction. Though not directly related to the thesis topic, this section does give a good idea of the various approaches adopted by researchers to overcome the stiction problem at the release stage and eventually in-use stiction. Section 2.3 summarizes various other proposals to overcome the problem of friction and in-use stiction.

2.2 Release-related stiction

As mentioned in Chapter 1, release-related stiction occurs during the final rinsing stages of the sacrificial oxide layer etch. This phenomenon occurs when the restoring forces are unable to overcome the interfacial forces like capillary,

electrostatic or van der waals forces. The following sections explain the approaches adopted so far to overcome this problem.

2.2.1 Freeze-Drying methods

Freeze-Drying methods came into picture when a high amount of failures during release of microstructures were attributed to the capillary forces developed after chemical wet etches. The rinse solution was first frozen and then subjected to sublimation. The capillary pull effect was eliminated by freezing the sample and then exposing it to a heated vacuum environment. Under these vacuum conditions, the frozen rinse solution is removed by sublimation [15].

Guckel and Burns were the first to apply this concept to the release of microstructures [16]. Freeze-drying concept however, has a few negatives which affect the yield of these devices. One of them being, a significant volume change experienced by the rinse solution. This volume change is sufficient enough to create stress thus leading to destruction of the device. The above mentioned authors used a cryoprotectant rinse solution consisting of methanol and water to reduce the volume change. Takeshima *et al* came up with a similar process, wherein they replaced the rinse solution with the sublimation liquid t-butyl alcohol which freezes at 26˚ C [17].

Kim *et al*, after conducting a series of experiments with sublimation liquids, t-butyl alcohol and p-dichlorobenzene, learned that t-butyl alcohol absorbs moisture when cooled below room temperature or when left open in the air for an extended period. After solidifying in the refrigerator, transporting the sample into a vacuum environment caused moisture condensation. Water introduced into the microstructure can hinder the sublimation process, rendering the device useless. High stress is often created in the solidified material owing to rapid solidification. This stress can severely damage constrained structures, while free moving structures like cantilever beams are less affected. Failures such as these were attributed to cracks formed in the solidified chemical or to the structure's inability to comply with the overall shrinkage of the chemical.

2.2.2 Dry Etching

Several dry etching techniques have been proposed in order to overcome the problems faced due to wet chemical etch techniques. Though these techniques seem to eliminate the surface capillary forces, the choice of etchants remains difficult. One of the reasons being that to etch silicon dioxide, strong etchants which do not have good selectivities with respect to the structural elements are required. Vapor-phase HF seemed to be a suitable candidate for the dry release of these surface micro-machined devices. This technique had the problem of water condensation, which was difficult to avoid because of the water molecules that were formed as a result of the chemical reaction. This seemed to be a significant problem with vapor-phase HF etching.

Lee *et al* [18] suggested that by etching the sacrificial silicon dioxide using hydrofluoric (HF) vapor instead of the aqueous HF solution, the need for subsequent rinsing and an elaborate drying procedure is eliminated. They used an anhydrous mixture of HH/CH3OH under low pressures to solve the problem of water condensation. Using Methanol (CH3OH) instead of conventionally used water vapor helped in avoiding the water condensation and formation of other residues. HF and Methanol mixture was physically adsorbed on the silicon dioxide surface during etching. The final byproducts of the chemical reaction are removed from the surface by desorption. The most significant reaction is the ionization of HF molecules. The oxide etch rate was shown to be proportional to the ionization reaction rate. The authors also noted that vapor-phase etching was much slower compared to wet chemical etch techniques. Methanol/HF vapor mixture also seemed to release much longer polysilicon beams than HF/water vapor mixture.

Vapor phase HF etching however, at elevated temperatures also exhibited a high rate of attack on silicon nitride films [16]. Several techniques were proposed to replace the sacrificial layer by polymers, which could later be etched by etchants less harmful to the silicon-based materials. O2 plasma or ozone, known to be milder on the structural material could etch these plastics. The microstructures could also be released through plasma if the sacrificial layer is silicon.

Many of the plasma etch processes use fluorine containing gases or gas mixtures. These fluorine atoms produced by the plasmas actually form the main reactants to perform isotropic etching. But the ions and molecular radicals produced by the plasma environment can adversely affect the substrate in some device applications. A plasmaless gas which can react with Si and which is highly selective on SiO2 circumvents the above problems. Xenon Difluoride (XeF2) was found to be a suitable plasmaless etchant which etched silicon effectively but maintained infinite selectivity on Silicon dioxide. Lbbotson *et al* showed that isotropic silicon etching over silicon dioxide could be done more selectively with halogen fluorides than with plasma generated fluorine atoms. Also, the etch rate could be independently controlled either by the partial pressure of the reactant or the temperature whereas, the reaction rate in case of plasma was much more difficult to control. However, the surface morphology was shown to be the same whether Fluorine atoms, halogen fluorides or Xenon Difluoride were used.

Qi Wang *et al* studied gas phase silicon etching using Bromine Trifluoride (BrF3) at room temperature. They observed consistent etching results and high molecular etching efficiency by performing etching in a controlled pulse mode. The gaseous BrF3 was found to have good selectivity over silicon dioxide, silicon nitride and photoresist. BrF3 etching process was also shown to be used in the release of micromachines, where silicon nitride was used as a structural material and polysilicon as the sacrificial layer [19].

2.2.3 Drying process using Magnetostatic forces

Lui *et al* presented a novel way of drying wherein the surface microstructures are lifted from the substrate during the liquid removal process to avoid stiction. Electroplated Permalloy material is used to provide the torque to the microstructure through an external magnetic field. In many MEMS applications like fluid control and optical systems, these micromachines must have sufficient surface area. And the risk of stiction during release for such microstructures remains high. The authors integrated a magnetic thin-film with the microstructures, which contained thin-film

plates and support beams, both of which were made of non-magnetic materials. The magnetic torque, created by the magnetic thin-film and an external field tends to align with the field lines. Thus, the microstructure and the substrate are actively separated by the torque during the drying and this prevents adhesion between the two surfaces. The magnetic field is removed after the rinsing stage is complete, and the microstructures are returned to the substrate plane. The above mentioned method had the following advantages. First, it could satisfy the requirements of large displacements and large forces. Second, it could be achieved globally using an externally applied magnetic field, thereby improving the efficiency when a large number of microstructures are fabricated.

The thin-film Permalloy material is not magnetized when the external magnetic field is zero. However, the internal magnetization develops within the Permalloy once the external field is applied, the orientation of which is within the plane of the structure. The magnetization has a linear relationship with the magnetic force and increases with the magnetic force applied. For equilibrium conditions to be achieved, the torque acting on the Permalloy should equal the sum of the structural deformation and the surface tension forces. Although the integration of a magnetic material adds one more step to the fabrication process, the drying stage remains fairly uncomplicated and does not involve any complex chemical or mechanical solutions. Also, the Permalloy material was shown to withstand the HF etch without much damage.

Drying using Magnetostatic forces prevents stiction because levitation force counteracts the surface tension force so that the microstructures and the substrate never come into contact. The success of the above mentioned technique requires a much more detailed studies and experimental observation of the contact angles at the interface of the liquid and the microstructures. The surface micromachined structures are kept away from the substrate during the drying process to prevent contact between the structure and the substrate. This technique is intended to aid the existing anti-stiction methods, and certainly proves well for micromachines with large surface areas. However, this technique is limited to cases where microstructures can achieve angular deflection [20].

2.2.4 Photoresist-assisted release of microstructures

This technique employs a grid pattern of photoresist which reinforces the microstructures during the wet chemical etch followed by rinsing and drying. This photoresist is eventually removed by a dry process. Kobayashi *et al* employed this technique to fabricate comb-drive micro actuators and demonstrated a considerable yield [21].

The microstructures are anchored to the substrate with a photoresist grid pattern during a typical release procedure – wet etching, rinsing and drying. This photoresist grid supports the microstructures against liquid movement during the wet etching process and against the capillary pull forces during drying. The photoresist eventually is removed by a dry process, thus preventing adhesion of the free microstructures onto the substrate. Instead of typically removing the sacrificial silicon dioxide, the layer is anisotropically etched by using the patterned polysilicon on top as a self-aligned etch mask. The remaining silicon dioxide is then undercut by dipping in hydrofluoric acid (HF). A thick layer of photoresist (PR) is then spin coated, exposed and then developed to form PR structures. Compliant microstructures such as cantilever beams have multi-footed bridge structures with the PR grid during the crucial release steps. This photoresist grid is then removed by oxygen plasma in a dry process to form free moving microstructures.

Photoresist release of microstructures is an add-on to the already existing process. This process supports the microstructures against surface tension before being removed by a dry process in the last step. It converts a normal wet-release into a dry release by the addition of a PR layer. However, in addition to the existing typical surface micromachining process, this technique requires additional steps like anisotropic sacrificial layer etching, photoresist (PR) spin coating including exposure and developing, and photoresist ashing.

2.2.5 Liquid bridge cleavage

During the release process, the capillary forces cause the microstructure to collapse because the liquid volume tends to concentrate near the weakest central part

of the microstructure. This can be avoided if the liquid volume is made to concentrate near the anchors instead. Abe *et al* patterned a sharp corner near the weakest point in the structure, thus breaking the liquid bridge into two separate droplets that tend to reside near the anchors. This technique can be used to release long beams without the need of complicated techniques [16]. The above mentioned authors worked on the principle that the shape of the microstructure periphery played an important role in the drying process. They concluded that by adding small areas with convex corners to the periphery of microstructures, near the point of largest vertical deflection, stiction could be considerably reduced in the post release-etch processing [22].

2.2.6 External Force

Structures that are adhered to the substrate in the post release-etch processing can be freed by applying external force. Samples can be freed by applying a small shear force, usually with a probe tip [16]. Gogoi *et al* thought of a technique which used Lorentz force due to the interaction of a current with an external magnetic field, to generate an upward force that frees the adhered microstructures [23].

The technique consists of patterning a conducting wire on top of the microstructure, which will carry a current along it. The microstructures, which are placed in a traverse magnetic field applied by an external magnet, are then electrically probed while current is circulated through the wire. The interaction between the current and the magnetic field generates a lifting force due to Lorentz effect. If this current is sufficiently large, the lifting force peels the microstructure until it is completely released. But the main difficulty with the above mentioned technique is the construction of the wire which may cause unnecessary warping of the suspended member.

2.2.7 Differential adhesion methods

Smela *et al* developed an alternative release method based on differential adhesion. Sacrificial layers are normally used in surface micromachining processes to

facilitate the movement of structural parts that are attached to the substrate. Silicon dioxide is the sacrificial layer generally used in the surface micromachining process, which is then etched away during the release process. There are several disadvantages associated with this. One of them being the damage of structural materials by the etchants used to remove the sacrificial layer. And in some cases, it may be difficult to remove the sacrificial layer completely.

The above mentioned authors developed an alternative method to release the micromachines, allowing them to pull themselves off parts of the surface. The fabrication method is as described. A thin layer of chromium, to which gold adheres well, is deposited first. For the second layer, the authors deposited and patterned an inert rigid polymer. When the completed device was operated, the tensile stress generated by the polymer pulled the gold and the underlying rigid plates free from the silicon, but the polymer layer remained attached through the chromium. The main advantage of this method is that it eliminates the need to protect layers during the chemical etch, and frees structures without the problem of adhesion [24].

2.2.8 Supercritical CO2 drying

Supercritical CO2 release of microstructures has shown to result in dry microstructures without collapse, unlike the conventional drying techniques which have been plagued by stiction and collapse of the structures onto the substrate. Substances have a critical temperature and a critical pressure and the point at which the critical temperature and pressure intersect is called the critical point. The critical point of CO2 is at 31ºC and 72.8 atm. Substances which go above their critical point are said to be supercritical. When substances tend to reach their critical point, they seem to exhibit properties that are both gas-like and liquid-like. Their liquid-like properties include transport and dissolving like that of a liquid, though they are much denser than gases. Also, their gas-like properties include low viscosity and little or no surface tension. These properties make supercritical CO2 an ideal candidate for the release of micromachines [25].

Supercritical CO2, because of its low surface tension property is especially attractive for the release of high-aspect ratioed surface micromachined structures. After the cleaning step, no rinsing or drying is required since supercritical CO2 completely evaporates upon depressurization to atmosphere [26].

The supercritical fluid, because of its negligible surface tension, has unabated access to solvent residing in capillary like spaces under the micromachined structures. Carbon dioxide is known to be a good solvent for many organic compounds especially methanol, which is used in the release process of micromachines. After the methanol has been dissolved and carried away by the supercritical fluid, the vessel is depressurized to yield dry microstructures.

Russick ***et al*** demonstrated that supercritical carbon dioxide could reliably extract methanol from all the microstructures that were tested. Test samples were supercritically extracted as follows. The micromachined samples were transferred from a methanol bath to a sample trough, which in turn was loaded into a vessel pressurized with CO2. After extraction, the vessel was depressurized and samples were removed from the extraction vessel [27].

2.2.9 Self Assembled Monolayer (SAM) coatings

Several researchers have been working on avoiding the stiction-related problems during release through chemical modification of the surface. One of these techniques include the Self-Assembled Monolayer (SAM) coatings. Self-Assembled Monolayers were introduced in the technique of releasing the MEMS devices because of their hydrophobic property. They are ordered molecular assemblies formed by the adsorption of an active surfactant on a solid surface. These monolayers are formed by the self-assembly of the surfactant molecules on the surface.

Self-Assembled Monolayers are known to eliminate the release stiction by effectively reversing the shape of the water meniscus, which forms underneath the microstructures during drying [28]. The capillary pull becomes a push if the contact angle is made more than 90^{o}. Several researchers have been studying the contact angles of aqueous solutions on Si and SiO2 surfaces, and oxidized surfaces are shown

to be hydrophilic with contact angles ranging from 0º - 39º. Though bare silicon (Si) surfaces cleaned of native oxide using HF were hydrophobic, chances that native oxide would regrow with exposure to water or air are pretty high. Complete hydrophobicity is thus difficult to achieve. Chemical modification of the surface is required to accomplish higher contact angle [16].

A number of well known hydrophobic Self-Assembled Monolayers have been grown on Si surfaces with good results. SAMs of alkylchlorosilanes, alkylalkoxysilanes, and alkylaminosilanes require hydroxylated substrates for their formation. The ***in-situ*** formation of polysiloxane, which is connected to the surface silanol groups (-SiOH) via Si-O-Si bonds, is the driving force for self-assembly. The hydrophobic layers are based on the silanization of silicon surfaces with organic groups by treating the surface with octadecyltrichlorosilane (OTS) precursor molecule. This procedure first involves the replacement of the aqueous rinse solution with an organic solvent through a series of steps. Self-Assembled Monolayer coating is given and then the solvent is replaced by water through a series of reverse dilution steps. Since these silanized surfaces have contact angle of approximately 114º, rendering the surface hydrophobic, the water recedes from the surface resulting in a dry sample [16]. Srinivasan ***et al*** improved the quality of the release method by using perfuorinated alkyltrichlorosilanes SAMs formed using FDTS, which seem to have better thermal stability compared to OTS [29]. Apart from effectively eliminating the release stiction in the drying process, these SAMs are also known to reduce in-use stiction considerably.

2.2.10 Fluorinated coatings

Fluorinated hydrocarbon coatings consisting of CFx chains are also likely candidates because of their low-surface energy. Plasma polymerization is a common way to grow these films. These films are shown to display little wear and remain hydrophobic even at elevated temperatures [16].

2.3 In-use stiction

In-use stiction comes into picture during the working of micromachines, after their release. It is the adhesion of free-moving structural parts to other mechanical parts or the substrate due to electrostatic forces or difference in electric potential. When these forces exceed the restoring forces, the mechanical parts are permanently stuck leading to damage of the device. Researchers have been working on techniques to reduce the in-use stiction and friction. The following are some of the procedures adopted in an effort to alleviate the above mentioned problems.

2.3.1 Surface modification

Adhesive forces can be reduced considerably if the contact area between the micromechanical structure and the substrate is reduced. Yee *et al.* suggested a surface modification technique to reduce the sticking problems in surface micromachined devices. This technique realizes very rugged surface at the substrate polysilicon, resulting in reduced sticking through a decrease in the real contact area. The surface consists of honeycomb shaped grain holes, defined by a two-step dry etch.

The above method alleviates the surface energy between the contacting surfaces by increasing the surface roughness of the substrate plane, without any additional photolithographic steps.

Following the deposition of polysilicon on the oxidized silicon wafer, the polysilicon is doped with phosphorous followed by thermal oxidation. Only the thicker oxide in the vicinity of the grain boundaries remains, while the oxide over the grains is completely etched back. This etch-back of oxide consists of the first step of the two-step dry etch to form the polysilicon grain holes. Polysilicon is then etched to complete the grain holes using the remaining oxide as a mask material. Surface roughness can be controlled, by varying the time for etching these grain holes. After the formation of grain holes at the substrate, a sacrificial oxide layer is deposited followed by the structural polysilicon layer. The sacrificial oxide layer is then etched isotropically followed by rinsing and drying. These samples could either be rinsed in DI water followed by drying at 200ºC in a conventional oven, or rinsed in methanol

followed by drying at 100ºC in a conventional oven. This technique aimed at reducing the contact area between the elastic member and the substrate and thus reported an increase in the detachment length by more than double [30].

The texturing can also be introduced by constructing an array of small supporting posts called ‘dimples’. These dimples are fabricated by etching small indentations into the sacrificial oxide layer before the deposition of the polysilicon structural layer. Dimples act as support for the suspended members and hence help in the reduction of stiction. But this technique cannot be used for microstructures with flat surfaces, and the adhesion of the dimple is larger than anticipated while drying out the sample.

Another technique to reduce stiction is the use of sidewall spacers. These sidewall spacers could be fabricated without additional mask steps and help in reducing the geometrical contact area.

2.3.2 Tungsten coating

Mani *et al.* [31], at the Sandia National Labs came up with an approach of selectively coating the micromechanical structures with tungsten to reduce adhesion and friction in these structures. This approach is manufacturable since chemical vapor deposition (CVD) of tungsten is used in the integrated circuit (IC) industry.

The above mentioned authors demonstrated an improvement in the wear characteristics of micromachines with much less process impact. The selective deposition of tungsten is achieved through silicon reduction of WF6, which results in a self-limiting reaction. Tungsten is selectively deposited after the removal of the sacrificial oxide layer. Since the deposited tungsten infiltrates under adhered silicon parts, adhered parts that are contacted over small areas such as dimples are also released. Tungsten has attractive properties as a wear resistant. It is hard, unlike many of the polymeric coatings used, which only have a low co-efficient of friction. Tungsten is also resistant to temperatures typically associated with packaging and is ultra high vacuum compatible.

When WF6 encounters heated silicon, a reaction occurs in which SiF4 or SiF2 gas is formed and W is deposited on the silicon surface. Once a continuous film of tungsten is formed, the reaction stops since WF6 is now shielded from silicon. Also, this reaction does not occur on silicon dioxide or silicon nitride. The above mentioned authors used microengines to assess wear and reliability. The tungsten coating showed improvements in the wear characteristics. Microengines coated with W showed longer lifetimes than polysilicon microengines in the experiments conducted. Tungsten coating was shown to change the mechanical behavior of the polysilicon structure, while satisfying the MEMS device requirements and not influencing the device performance.

2.3.3 Fluorocarbon bumpers

Kozlowski *et al.* came up with a novel idea to avoid the sticking of fabricated structures to the substrate during operation after an accidental touch, by building bumpers under these structures. These bumpers are designed to keep the free-moving structures in distance from the substrate.

The free-moving structures could adhere to the substrate even after release during their operation. One of the reasons would be the humidity in the surrounding air, which forms a thin layer on the surface of the structure and the substrate, causing them to stick when they come into contact. In order to avoid this, the above mentioned authors deposited water repellent fluorocarbon bumpers. The authors tried depositing the fluorocarbon layer through the holes of the punched membranes. The idea was to form a fluorocarbon layer using an appropriate bias voltage, so that the molecules hit the surface at an angle between 90º - 70º. The fluorocarbon bumps were deposited in a reactive ion etcher (RIE). Thus small fluorocarbon bumps are formed below the holes, with diameters slightly larger than the holes. Hence, an accidental deflection of the membrane towards the substrate will only lead to a contact at the edges and does not result in sticking [32].

2.3.4 Ammonium Fluoride anti-stiction treatment

This technique is a surface treatment for stiction reduction, which has shown to passivate the surface micromachined mechanical microstructures. Houston *et al.* [33] achieved surface passivation during etching of silicon by ammonium fluoride (NH4F) by means of a high quality hydrogen-termination of surface dangling bonds.

The above mentioned technique integrates the NH4F treatment directly with conventional release processes. The approach is to reduce the attractive forces acting between the microstructure and the substrate by altering the surface properties. Since hydrophobic surfaces will necessarily have lower surface energies, they exhibit low Van der Waals as well. The elimination of the electrically insulating and charge trapping oxide layer on the silicon surface should promote charge dissipation upon contact, thus reducing electrostatic forces. Hydrogen terminated silicon (Si-H) surface is chosen here, which is produced by etching in ammonium fluoride.

During the etch process, HF is known to etch silicon dioxide down to Si/SiO2 interface, and this leaves a predominantly hydrogen-terminated surface, which are then treated with ammonium fluoride. The NH4F treated surfaces are thought to be superior to the HF surfaces, due to a more complete hydrogen termination, leading to a cleaner and more hydrophobic surface. Also, small pyramidal protrusions are formed after this treatment, roughening the surface. This could also be one of the reasons for stiction reduction.

The work of adhesion was measured using an array of cantilever beams. The work of adhesion was shown to be reduced by two orders of magnitude in case of micromachined mechanical structures treated with ammonium fluoride. The rough, grained surface of the polysilicon also reduced the work of adhesion on these surfaces compared to perfectly smooth surfaces. But the Si-H surface produced by ammonium fluoride is metastable in air, where oxidation begins to take place within a week of exposure to air.

Though the work indicates the ability to lower in-use stiction, through tailoring of specific surface properties, it does not allow successful operation in room air. Hence, the most critical aspect of successful encapsulation process will be providing a dry atmosphere or vacuum for the released structures.

2.3.5 Alkene based monolayer films

Another class of anti-stiction coating for the silicon based microelectro mechanical systems is the technique based on free-radical reaction of a primary alkene (e.g. 1-octadecene) with hydrogen terminated silicon. Ashurst *et al* [34] claimed that this new monolayer coating had several advantages over the other self-assembled monolayers (SAMs) i.e. OTS (octadecyltrichlorosilane) and FDTS (perfluorodecyltrichlorosilane).

The above technique is based on controlling both the topography and chemical composition of the contacting surfaces during operation of the micromachines, in order to alleviate in-use stiction and friction. It abandons the chlorosilane chemistry and adopts a free radical reaction of a primary alkene to bind the precursor molecule to the hydrogen terminated silicon substrate. The authors have used the reagent 1-octadecene C16H33CH=CH2, which does not produce HCl during the reaction. Also, there is no oxidation on the surface since the molecule binds directly to the silicon. The alkene is found to be stable at room temperature and insensitive to ambient humidity.

Silicon surfaces are hydrogen terminated after the sacrificial layer etch. The structures are then rinsed with 1-octadecene, and transferred to a reactor containing the 1-octadecene coating solution. The reactor is then heated to generate free radicals, during which monolayers are formed. Contact angle was found to be the same as in OTS. The above mentioned authors used sidewall friction testers to determine the co-efficient of static friction. The results showed that the anti-stiction properties of films produced by alkene chemistry are comparable to those produced by the trichlorosilane SAMs, but without their limitations. This technique does not produce any HCl during the reaction whereas chlorosilane-based chemistry does. Also the coating process is more robust since it is insensitive to relative humidity, and the coated surface has much fewer particulates compared to that of OTS. Moreover the coating process can be made selective to coat only the exposed silicon by generating radicals using a radical initiator. However, thermal annealing of octadecene films in vacuum has shown to produce silicon carbide.

2.3.6 Conformal fluorocarbon coatings

Anti-stiction coatings need to be hydrophobic, with contact angle more than 90º in order to preclude in-use stiction. Also, these coatings need to be conformal enough to cover all the hidden surfaces of these micromechanical structures. Anti-stiction coatings of fluorocarbon (FC) were studied by Man *et al.* to alleviate the in-use adhesion in microstructures. The goal was to find a coating, which was thick enough to withstand vaporization, wear and friction, yet, thin enough not to disturb the mechanical nature of the microstructure.

This technique aims at forming a conformal fluorocarbon coating through plasma polymerization of decafluorobutane (C_4F_{10}) on a field free zone. The whole mechanism consists of initiation and propagation. This occurs when the plasma is ignited and the monomers generate reactive species, which are either ionized or neutral. Once the reactive species are generated, they react with other reactive species to form larger molecules. This process continues until they are heavy enough to deposit on the substrate. However, not all kinds of fluorocarbons polymerize, some of them undergo etching. The condition where polymerization occurs mainly depends on the fluorine to carbon ratio of the monomer. Also, the large surface mobility of the active species is one of the reasons for good uniform coating. Contact angle measurements were performed to evaluate the fluorocarbon coating's ability to serve as an anti-stiction layer, which was found to be 110ºC.

Samples coated with fluorocarbon coating were also subjected to durability tests like aging and accelerated wear tests, and were subjected to elevated temperatures like 400ºC. These tests predicted a lifetime greater than ten years at 150ºC. Periodic wear tests indicated that the coatings remain hydrophobic even after several contact cycles. The polymer coating remained hydrophobic without any evidence of noticeable degradation. Also, these films were found to prevent the adhesion of microstructures to their substrates even after direct immersion in deionized water. The conformality of the film was found to vary approximately between 10 –20% uniformity under the microstructure surfaces [35].

2.3.7 Self-assembled fluorocarbon films

Srinivasan *et al* [36] developed a fluorinated Self-assembled monolayer (SAM) coating process for stiction reduction in polysilicon microelectro mechanical systems that does not use chlorinated solvents. They studied the properties of FDTS SAMs on polysilicon beam arrays.

The SAM coating of silicon with RSiCl3 precursor begins with the hydrolysis of the head group to give 3 silanols (SiOH). These groups then condense with silanols on both the oxidized surface of silicon and other precursor molecules to give covalent siloxane crosslinks (Si-O-Si). The surface is composed of alkyl or perfluoroalkyl tailgroup after the monolayer formation. The FDTS SAM coating is done without the chlorinated co-solvents, since the kinetics of SAM formation from hydrocarbon or fluorocarbon precursors vary. In order to quantify in-use stiction, beams longer than 400μm were brought into contact with the underlying substrate by applying a voltage of about 150V to a narrow actuation pad near the anchor region. Shorter beams were depressed with a sharp tungsten probe tip. The lengths of beams that remained stuck to the substrate were then recorded. Sticking probabilities for each beam length and surface coating were calculated to find the apparent work of adhesion (W), the energy required to separate the two surfaces from contact.

Experiments pertinent to in-use stiction showed that the fluorinated SAM films reduce the adhesion to a value which is lower than four orders of magnitude than that of SiO2 coating. The length corresponding to 50% sticking probability for the FDTS coated films was found to be approximately 780μm, compared to 550μm of the OTS coated films. Also, the FDTS treated surfaces were found to survive heat treatment up to 400 C. In air, the thermal stability of fluorinated SAMs is considerably better than that of the hydrocarbons. A common path for hydrocarbon decomposition in the presence of water is through water attack and dehydrogenation. While the perfluorocarbons are also thermodynamically vulnerable to hydrolysis, they are found to be inert in air until heated to a temperature around 500 C.

This work also indicates that the roughness of contacting SAM-coated surfaces is critical to the level of stiction encountered.

2.3.8 Deposition of thin Teflon-like films

This technique is based on depositing thin Teflon-like films using commercial plasma like reactor to eliminate adhesion or stiction in already released microstructures. Smith *et al* [37] used a Lam384T oxide etch system in a remote plasma mode, with commercially available trifuoromethane (CHF3) to deposit thin hydrophobic films around and under the micromechanical structures. The above mentioned authors were successful in producing hard, uniform Teflon-like films which could penetrate under and over these structures.

When a fluorocarbon gas is placed in a plasma reactor, the gas is fractured into a 'plasma soup' of ions, excited molecules and radicals. Depending on the gases that are fed, substrates exposed to the plasma can be etched or have a polymeric film deposited on them. Polymerized tetrafluoroethylene can be grown if the fluorine to carbon ratio is approximately two. Ion impingement coupled with the short diffusion length of the plasma causes the fluorocarbon film to be deposited anisotropically. The substrate needs to be in a field-free zone adjacent to the plasma in order to make the film growth more conformal.

Sufficient film deposition was found in the undercuts of the microstructures, to make the surface hydrophobic. The contact angle measurements of 108º showed a hydrophobic nature whereas, the uncoated surfaces showed a contact angle of 61º. The refractive index of this film was found to be around 1.4. The refractive index and contact angle indicate that the film is very similar to bulk Teflon pTFE, and these Teflon like films can be removed easily with oxygen plasmas.

The authors also conducted experiments to study the co-efficient of friction and wear lifetimes in these mechanisms, after the deposition of the Teflon-like film. These involve the acquisition of gear position versus time data, under the influence of specified drive signal to the microengine. The experiments show that the co-efficient of friction is reduced by an order of magnitude when compared to microstructures with no friction reducing coating.

2.3.9 Lubrication using bound and mobile phases of Fomblin Zdol

Eapen *et al* [38] studied the lubrication scheme for MEMS electrostatic lateral output motors based on a mixture of bound and mobile lubricant. They conducted tribological studies on Si (100) wafers, as well as MEMS motors, dip coated with a mixture of bound and mobile phases of Fomblin Zdol. Lubrication by bound monolayer alone provided an increase in the operational life of these microstructures, but in time these coatings wear off exposing the uncoated surface which eventually leads to the device failure. In order to obtain effective and long-term protection and lubrication, chemically bound species should be supplemented with a means of replenishment, such as the use of mobile phase that can migrate to the exposed areas and provide further protection.

Zdol is one of the perfluoropolyalkylether (PFPAE) lubricants. The sample used for the experiments had an average molecular weight of approximately 2000 amu. Zdol is a bifunctional PFPAE with terminal CH2OH groups. The hydroxyl groups can react with either Si-OH or Si-H groups on the silicon surfaces to establish covalent bonds. Studies on Fomblin Zdol by Ruhe *et al* [34] have shown that it can provide both chemically bound and physically adsorbed species on a model silicon surface, the latter acting as a mobile phase.

Thin lubricant layers were applied on the wafers and MEMS devices by dip coating from dilute solutions. A ball-on-flat tribometer was used for accelerated friction and wear tests. Experiments on the ball-on-flat tribometer were considered failed when a visible scar appeared on the Si surface. An ellipsometer was used to measure the thickness of films on Si surfaces. All samples coated with 0.5% of Fomblin Zdol showed lower values of friction co-efficient compared to the uncoated samples. A denser, thicker deposit was observed as the temperature was increased, increasing the covalent bond formation. But a dense bound phase, however, does not necessarily lead to better performance as evidenced by poor performance of wafers containing bound phase of Zdol alone.

However, the studies also showed that dip-coating of MEMS devices lead to non-uniformity in coverage, which may be caused due to the coating process itself or due to processes that occur during storage.

CHAPTER 3

EXPERIMENTAL APPARATUS AND PROCEDURE: QUARTZ CRYSTAL MICROBALANCE

3.1 Introduction

In this chapter, I will explain the apparatus used, circuits designed and the experimental procedures adopted to study the uptake of vapor phase lubricants on Silicon (Si) surface using Quartz Crystal Microbalance (QCM).

3.2 Study of uptake of lubricants on the Si surface

The purpose of this work is to study the change in friction and stiction characteristics in MicroElectro Mechanical Systems, after screening vapor phase lubricants in ultra high vacuum conditions. The test structures used here are the Sidewall tribometers specially designed to test friction, by Sandia National Labs. The uptake of these vapor phase lubricants on Si surface is first studied using Quartz Crystal Microbalance (QCM), the possible candidates are then screened on the test structures to study the effects of friction and in-use stiction. The experimental tools and procedures are described in the following sections.

3.2.1 Quartz Crystal Microbalance (QCM)

The Quartz Crystal Microbalance has been used for a long time to monitor thin film deposition either in vacuum or in gas. It is a well established tool for monitoring the adsorption of materials onto surfaces. Quartz is a crystalline form of SiO_2 that has a solid-solid phase transition at 573º C [38]. The basis of the QCM is the piezoelectric quartz crystal, which oscillates at a resonance frequency determined by several factors, including the mass of the crystal.

The QCM consists of a thin disk of single quartz crystal, the two faces of which are plated with metal electrodes. When an alternating voltage is applied across the electrodes, the QCM is made to oscillate mechanically at its resonance frequency. It has a relatively high quality factor and high frequency stability. The way a quartz crystal is cut has an impact on the crystal frequency as well as its stress and temperature responses. The AT- and BT- cuts are oriented at angles of $\theta = 35º\ 15'$, and $\theta = -49º$ respectively from the ZX plane. The following figure shows a basic quartz crystal microbalance design, which consists of AT-cut crystalline quartz, with gold electrodes on either side.

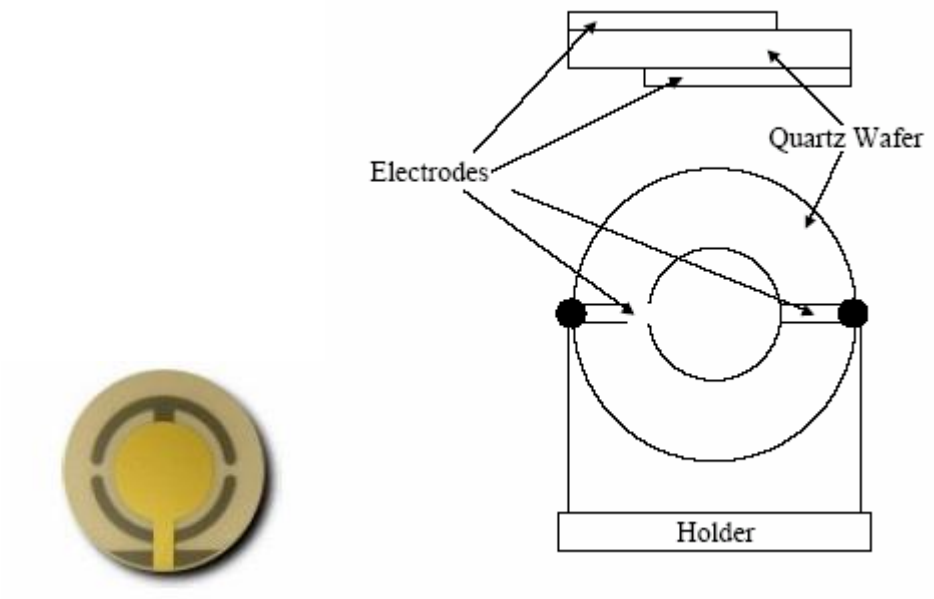

Figure 3.1. The Quartz Crystal Microbalance [39]

Since the AT-cut crystals have zero temperature coefficient near room temperature, they seem to be the most popular choice for a variety of applications. They also have higher frequency stability and mass sensitivity, hence are used in all the experiments conducted in the study.

For a given AT plane, the resonance frequency depends on the film adsorbed onto the crystal. More precisely, a thin rigid film, uniformly deposited onto the electrode surfaces, causes a drop in the frequency, $-\Delta f_{ads}$, equal to,

$$-\Delta f_{ads} = (4 f_{res}^2 / Z_q).(m/A)$$

where Z_q is the transverse acoustic impedance of the quartz ($Z_q = 8.862X10^6$ kg/m^2 s), m the mass of the film and A, the area of the electrode. The acoustic impedance Z_q is defined by the product $Z_q = \rho v$, ρ being the quartz density and v the wave velocity [40]. The following figure shows the crystal cut used for high-frequency thickness-shear mode of oscillation.

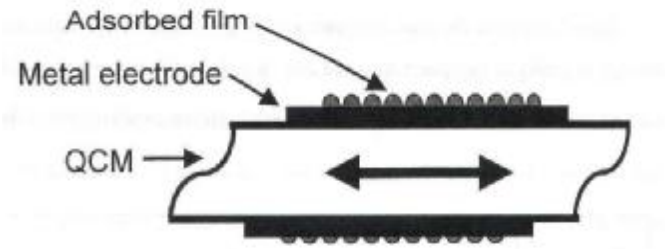

Figure 3.2. The QCM fundamental, thickness shear-mode, Oscillation [41]

In this study, the focus is on the use of QCM as a probe for sliding friction. J.Krim and Widom [42] developed this technique in 1986-88, where they were able to show through acoustic impedance calculations, that if a film slips on the surface of QCM, its sliding friction could be related to the damping of the crystal's oscillation. They also showed that amplitude shifts were due to frictional shear forces exerted on the surface electrode by the adsorbed film [43].

The driving force for the quartz crystal has a constant magnitude and is periodic, and is supplied by a Pierce oscillator circuit. The output from the pierce oscillator circuit is mixed with a reference signal using a mixer circuit. The mixer output which contains both the sum and difference frequencies of the two inputs, is fed into a low pass RC filter to filter out the higher frequency. The output of the RC low pass filter and its amplitude is directly proportional to the amplitude of the experimental crystal. The entire Quartz crystal Microbalance setup is housed in an ultra high vacuum environment. The lubricant is heated and screened in the form of vapor phase over the three quartz crystals. Crucibles fit into tungsten baskets serve as the thermal source for the lubricant.

The vapor phase lubricant samples are first studied using the Quartz Crystal Microbalance technique. Promising candidates are then screened onto the MEMS structures (Friction testers) to study the friction characteristics.

3.2.2 QCM Crystals

The first set of experiments are conducted on the Ag (Silver) coated, commercially (*Crystek Corp*.) available quartz crystals to study the conformality of the vapor phase lubricant. The uptake of this vapor phase lubricant on Si surface is then studied using a quartz crystal coated with Si. These QCM crystals are AT-cut crystals obtained from *Maxtec Inc.* (CA), having a cut angle between 35º14’ and 35º22’. The Silicon crystals are 99.999% pure vacuum deposition grade, having a thickness of 1000 Å of Si layer deposited on top of 2900 Å Au (Gold) layer, which in turn was deposited on a 400 Å Cr film. The crystals are then fitted into a pair of metal spring clips, which are mounted on an insulated base. These crystals were prepared by Yazan Hussain, Chemical Engineering department.

3.2.3 Pierce Oscillator circuit

The pierce oscillator circuit is used in this study to drive the experimental quartz crystals in the vacuum chamber. This circuit was chosen as it was found to be

convenient for a number of reasons. It works well despite high variable stray capacitances due to the long crystal leads and mounting arrangements. Its high frequency stability even at very low drive levels is another excellent advantage. Figure 3.3 shows the schematic of a pierce oscillator circuit.

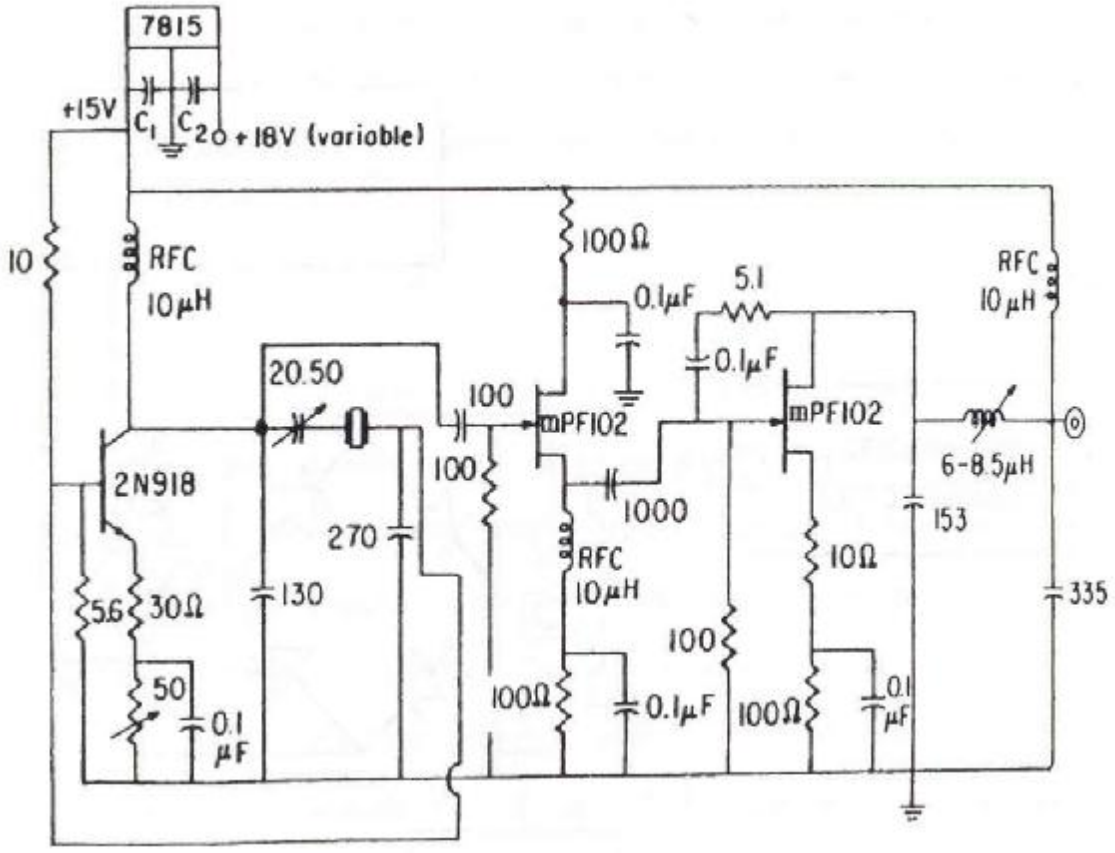

Figure 3.3. Schematic of the Pierce Oscillator circuit. [41]

3.3.4 Mixer electronics

The circuit employed in the data taking measurements gives simultaneous readings for the frequency and amplitude of oscillation of the experimental crystals. The pierce oscillator circuit is used to drive the experimental crystal, the QCM sample, whereas a reference frequency is got from a stable function generator. The two frequencies are then fed into the mixer circuit. This mixer circuit gives a signal

output containing both the sum and difference frequencies of the two input frequencies. This signal is then filtered with a low-pass filter. The resulting output is the difference frequency signal, $| f_{exp} - f_{ref} |$, whose frequency and amplitude is directly proportional to the amplitude of the experimental quartz crystal.

Figure 3.4 shows the schematic of the Mixer electronics circuit.

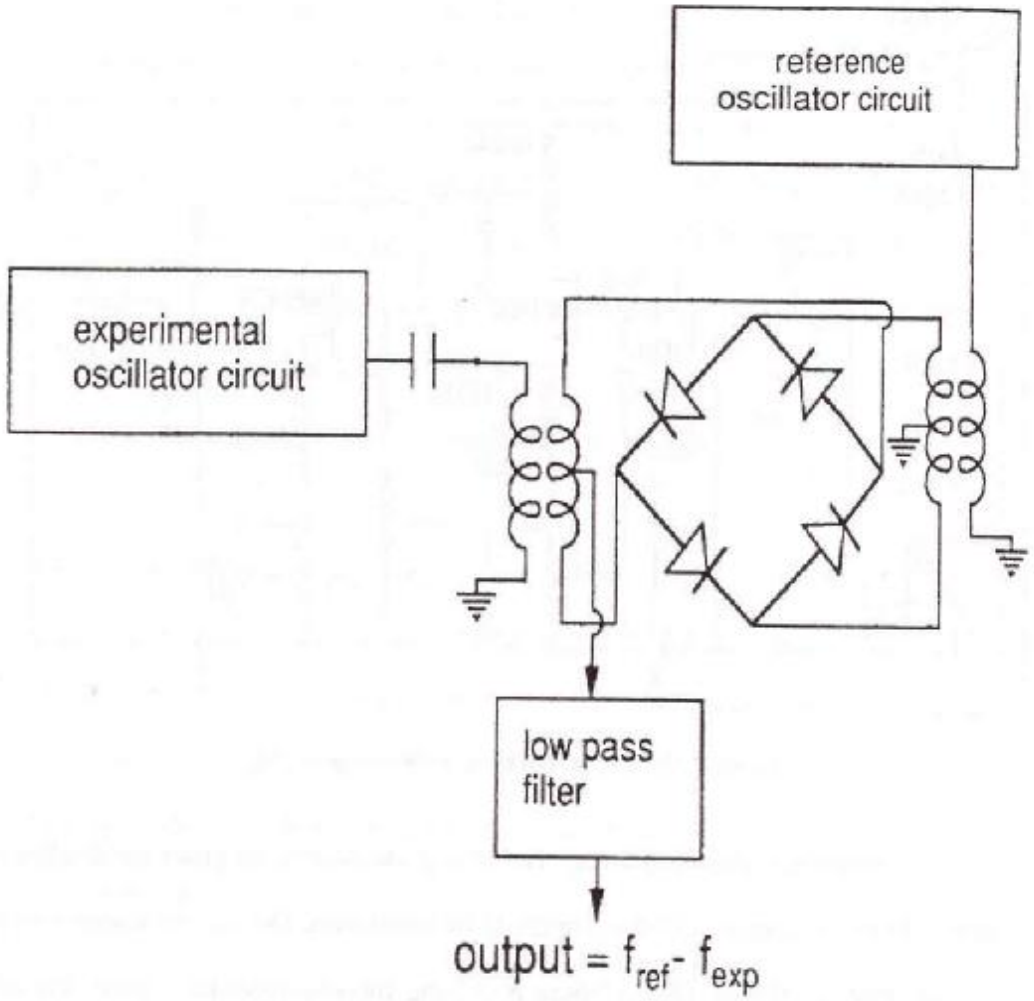

Figure 3.4. Mixer electronics circuit [41]

3.3.5 Ultra high vacuum setup for the QCM

The Quartz Crystal Microbalance is housed in the Ultra High Vacuum system while conducting the experiments. The UHV setup was built for ultra high vacuum compatible materials. However, the experiments were conducted in the range of 1.0 X 10^{-7} to 1.0 X 10^{-8} Torr, since the application did not require a ultra high vacuum environment. The UHV system helped in conducting the experiments in extremely well controlled environments, with the samples being atomically clean. At such low pressures, the contamination of samples is deterred considerably, thus allowing sufficient time to collect accurate data. All parts of the UHV setup are ultrasonic cleaned and baked at about 100º C for a period of 24 to 48 hours. Baking removes gas atoms which are stuck to the chamber walls, and which can inhibit the system from reaching low pressures. Figure 3.5 shows a photograph of the vacuum setup for the QCM experiment.

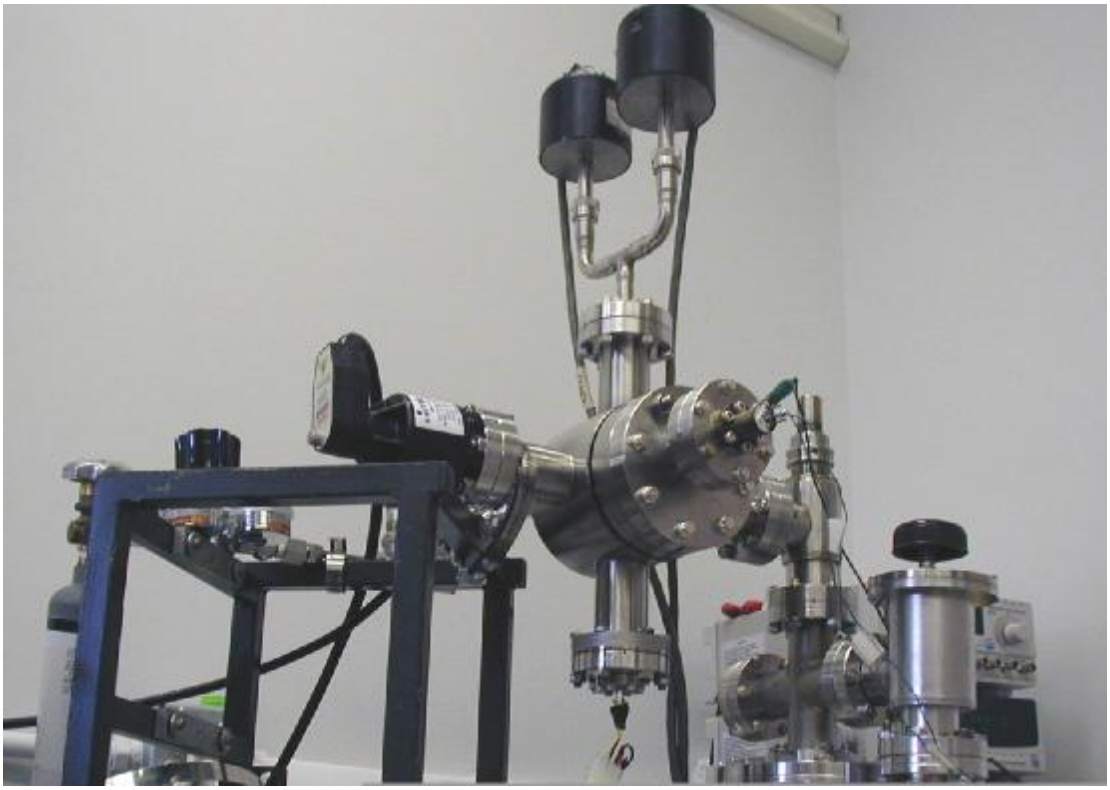

Figure 3.5. Photograph of the vacuum setup for the Quartz crystal microbalance.

The vacuum setup consists of a stainless steel chamber that contains an ion pump, sorption and turbo pumps, pressure gauge, quartz crystal holders, and the thermal sources for the lubricant sample. The thermal source consists of a crucible placed in a tungsten basket. The experimental chamber houses the three Quartz Crystal Microbalances. These three QCMs are evenly spaced to cover a significant portion of the chamber, to test the conformality of the vapor phase lubricant. The crystals are fed into the vacuum chamber using the electrical feed-through. The ceramic crucible is also housed in the vacuum chamber. A valve 'V1' connects the experimental chamber and the sorption and turbo pumps. This valve can be closed when the ion pump takes over at low pressures. These pumps are used to pump down the system starting from atmospheric pressure i.e. 760 Torr to about 1.0 X 10^{-5} Torr. After this stage, the ion pump which is connected to the experimental chamber takes over. The system can routinely reach a base pressure of about 1.0 X 10^{-7} Torr. Figure 3.6 illustrates the top view of the vacuum setup.

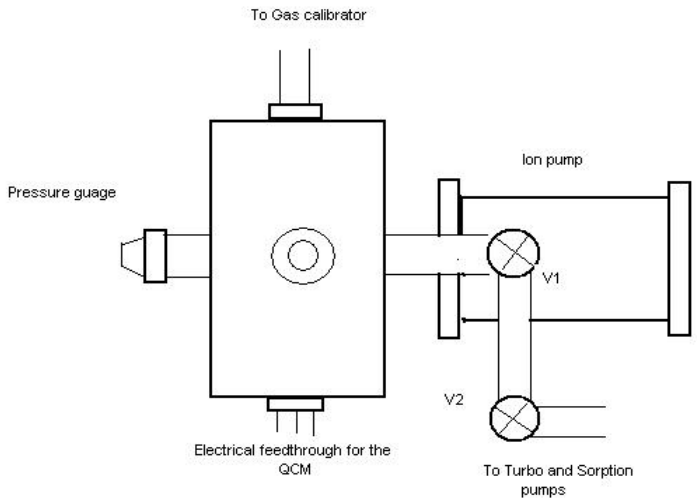

Figure 3.6. Top view of the vacuum setup.

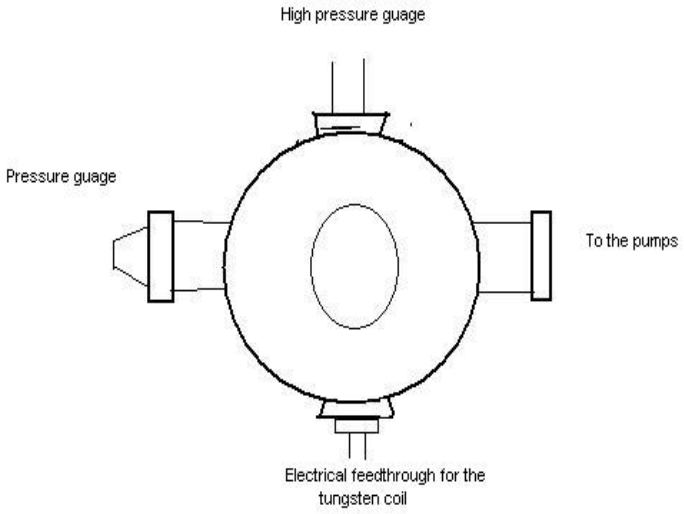

Figure 3.7. Side view of the vacuum setup.

CHAPTER 4

QCM EXPERIMENTAL RESULTS

4.1 Introduction

This chapter shows the results obtained from the Quartz Crystal Microbalance (QCM) experiment. Ideally, a vapor phase lubricant is required to have sufficient stability to be vaporized and transported onto the surface without decomposing, and it must not form deposits once consumed as a boundary wear film [51]. One of VPL's key advantages over conventional liquid lubrication is that a much less lubricant is required to provide a similar and, in many cases superior degree of frictional and wear reduction.

The lubricant used here is the commercially available t-butyl phenyl phosphate (TBPP) *Durad 620B* vapor phase lubricant, whose atomic constituents are carbon, hydrogen, oxygen and phosphorus. It has a viscosity of 125 mm^2/s at 40° C and a thermal stability of 282° C, exhibits oxidation inhibiting characteristics as well as a number of other desirable tribological properties, such as the reduction of wear. In the past, TBPP has been tested extensively in our group, and found to be a good choice of vapor phase lubricant. These phosphate esters vaporize onto active substrates to form tenacious, polymeric films compared to hydrocarbons which form loose flaky films. While the precise mechanisms for its beneficial properties are uncertain, it is believed that after reacting with the surface, the phosphate contained in the original lubricant molecule acts as a binder for graphitic carbon, which in turn may be the actual lubricant.

The QCM is particularly well-adapted for measurements of uptake rates of vapor phase lubricants. It has been used for decades for microweighing purposes, and was adapted for friction measurements in 1986-88 by Widom and Krim. Specifically, a QCM consists of a single crystal of quartz that oscillates in transverse shear motion with a quality factor near 10^5. The driving force (supplied by a Pierce oscillator circuit) has constant magnitude and is periodic with frequency f = 4 to 10 MHz, the series resonant frequency of the oscillator. Two metal electrodes, which serve as the substrates upon which adsorption occurs, are deposited in vacuum conditions onto each major face of the crystal.

Film adsorption onto the microbalance produces shifts in both the frequency and amplitude of vibration, which are simultaneously recorded as a function of pressure. Amplitude shifts are due to frictional shear forces exerted on the surface electrode by the adsorbed film (or alternatively by a three-dimensional vapor or fluid phase) [52].

4.2 Uptake of the lubricant on Ag surface

This set of experiments is conducted using the commercially available 8 MHz *Crystek Corp.* quartz crystals with silver electrodes, to test the conformality of the vapor phase lubricant. Three crystals are used, spaced such that the uptake of the vapor phase lubricant gives a fair idea of the lubricant's conformality. This property is essential, considering the fact that the MEMS devices are in the micrometer range, and in fact have crevices beyond the line of sight.

Two of the crystals are used with their encapsulation removed, while the other is used with the can (encapsulation) to test frequency drifts due to temperature variations. All three crystals are placed in the vacuum chamber, above the crucible containing the lubricant, held by the tungsten heating wire. The experiment is conducted at room temperature.

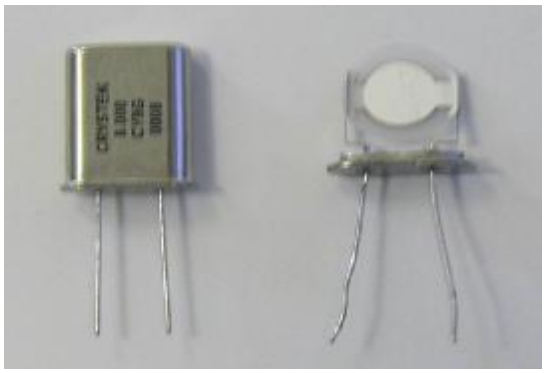

Figure 4.1. Schematic of the quartz crystals used.

Another set of experimental run is conducted. This time three crystals are used, two crystals with their can removed and the third one with a hole on the edge of the can. One of the open quartz crystals is placed horizontally above the lubricant source, such that only one side of the quartz surface is exposed to the vapor phase lubricant. This placement helps to understand whether the vapor phase lubricant can move around the crystal and deposit onto the other electrode. The other open quartz crystal is placed vertically, facing down, right above the lubricant source.

A number of routine checks are performed to assure good electrical contact between the crystal holder pins and the crystal tabs. Each crystal is connected externally to a pierce oscillator circuit, the output of which is mixed with a reference signal. The higher range of the mixed signal is then filtered. The vacuum system is then pumped down using a sorption pump, backed by a turbo pump. Once the pressure reaches 1.0×10^{-5} Torr, the ion pump is turned on, and the system reaches a base pressure of about 2.5×10^{-7} Torr. Once the system reaches this base pressure, the pumps are turned off to conduct the experimental runs.

The crucible held in the tungsten loop, within the experimental chamber is used to supply the lubricant in vapor phase. The tungsten loop current is increased gradually, to about 3 Amp, until the vaporization commenced.

Before each run, the QCM oscillation stability is checked. Then, simultaneous data of the experimental chamber pressure, frequency and amplitude of the QCM oscillation are collected. Each run typically lasts for about one hour.

Figure 4.2 shows the results of the QCM uptake results. The plot combines the results of the experimental runs. The analysis gives a fair picture about the nature of the vapor phase lubricant.

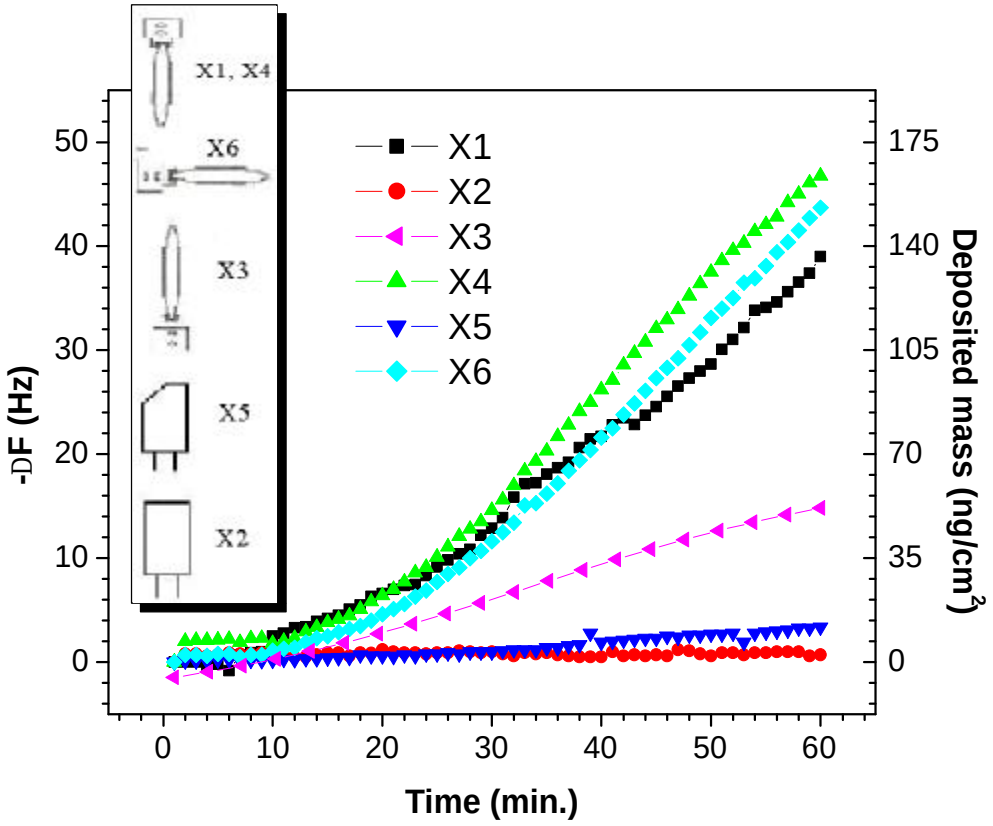

Figure 4.2. Frequency changes of the QCM of the 6 crystals during the lubricant uptake.

X1 and X4 are the plots of crystals (Crystal 1 and 4) placed vertically down, right above the VPL source. These plots show that the pattern of uptake is approximately same in both the cases. The change in frequency, $|-Df|$ Hz, in case of Crystal 1 is 38.98 Hz, and 46.75 Hz in case of Crystal 2. The mass deposited in these two cases are 134.60 ng/cm^2 and 161.42 ng/cm^2 respectively. X2 is the plot of the crystal, which was used to calibrate any temperature variations that might have caused the change in frequency during the experimental run. The plot shows that there were no such temperature variations.

X3 is the plot of the crystal placed vertical (facing up), away from the lubricant source in the vacuum chamber. This analysis is helpful in determining whether the vapor phase lubricant could travel far enough to deposit itself on the Crystal 3. The plot shows a frequency shift of 14.812 Hz, and 51.14 ng/cm^2 of mass deposition, which is approximately half of that of crystal 1. X5 is the plot of the crystal, whose outer can was kept intact except for a small hole drilled at the can's edge. This helped in knowing whether the vapor phase lubricant could make its way through the hole and deposit itself onto the crystal. The plot shows a frequency shift of 3.4 Hz, with a corresponding mass deposition of 11.74 ng/cm^2. This shows that even though the mass adsorbed is less, the vapor phase lubricant did deposit itself onto the quartz crystal. Plot X6 is that of crystal 6, which is placed horizontally, right above the lubricant source. As can be seen from Figure 4.2, this plot follows that of Crystals 1 and 4, proving that the vapor phase lubricant can actually move around the crystal and deposit itself onto the opposite electrode. The frequency shift in this case is 43.7 Hz and the mass deposited on this crystal is calculated as 150.896 ng/cm^2.

These analyses help in understanding the conformality of the vapor phase lubricant, and aid in comprehending the way the MEMS devices ought to be positioned in order to obtain well-lubricated devices.

4.3 Uptake of the vapor phase lubricant on Si and Si-OTS surfaces

This experiment aids in the study of the uptake of vapor phase lubricant on the Si and Si-OTS surfaces. Experiments were conducted on Si coated with OTS, since this silane is widely used during the release process of microstructures to overcome the problem of stiction. The QCM crystals used here are AT-cut crystals obtained from *Maxtec Inc.* (CA), having a cut angle between 35º14' and 35º22'. The Silicon crystals are 99.999% pure vacuum deposition grade, having a thickness of 1000Ang. of Si layer deposited on top of 2900Ang. Au (Gold) layer, which in turn was deposited on a 400Ang. Cr film. The crystals are then fitted into a pair of metal spring clips, which are mounted on an insulated base.

The crystal is placed vertical, so that the lubricant could be adsorbed on both sides. Routine checks are performed to ensure good electrical contact between the crystal holder pins and the crystal tabs. The experimental set-up is the same as explained in Section 4.2. The base pressure of the system while conducting the experiment was 1.8 X 10^{-5} Torr.

The tungsten loop current is increased gradually, to about 3 Amp, until the vaporization commenced. Before each run, the QCM oscillation stability is checked. Then, simultaneous data of the experimental chamber pressure, frequency and amplitude of the QCM oscillation are collected. Each run typically lasts for about one hour. Figure 4.3 shows the plot of TBPP uptake on two quartz crystals coated with Si film and one quartz crystal coated with Si which in-turn was coated with OTS (octadecyltrichlorosilane).

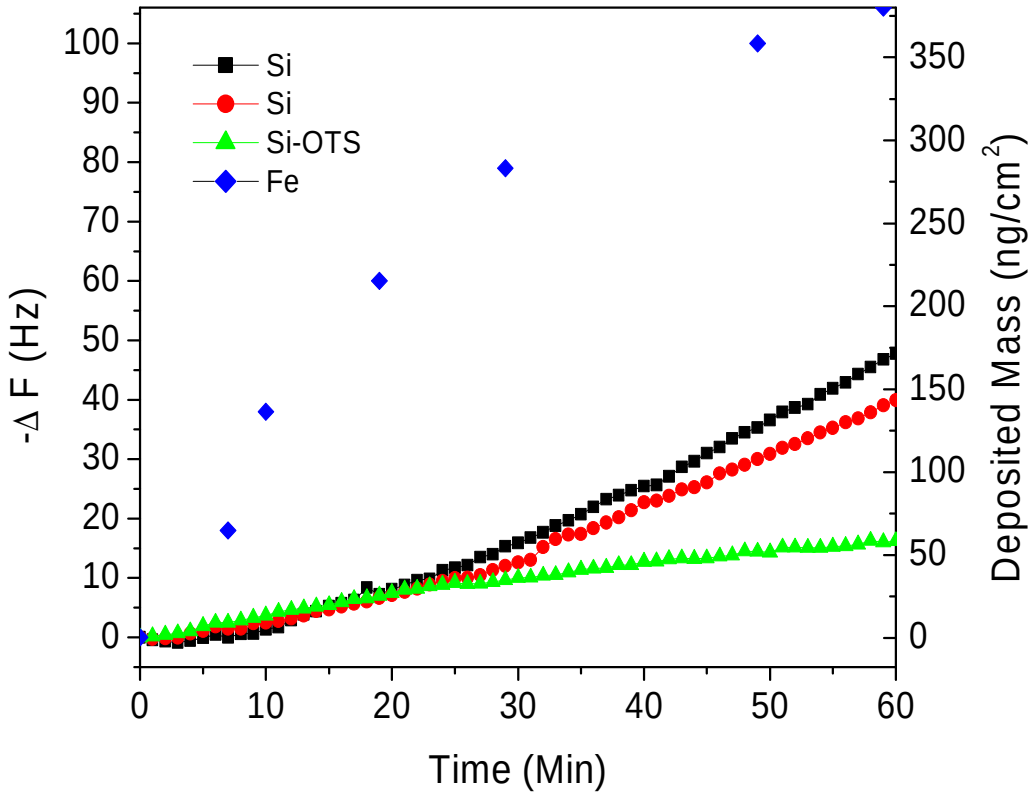

Figure 4.3. Frequency changes of crystals coated with Si film ,OTS on Si film and Iron.

The two quartz crystals coated with Si film show frequency changes of 47.8 Hz and 39.91 Hz respectively. The corresponding mass deposited being 165.05ng/cm^2 and 137.809 ng/cm^2. The uptake on Si-OTS is comparatively less, with a mass deposition of 55.90 ng/cm^2. The uptake of the vapor phase lubricant on Iron is also shown [52]. Figure 4.4 shows the amplitude shifts for the uptake of TBPP on Si-OTS surface, Si film and Iron.

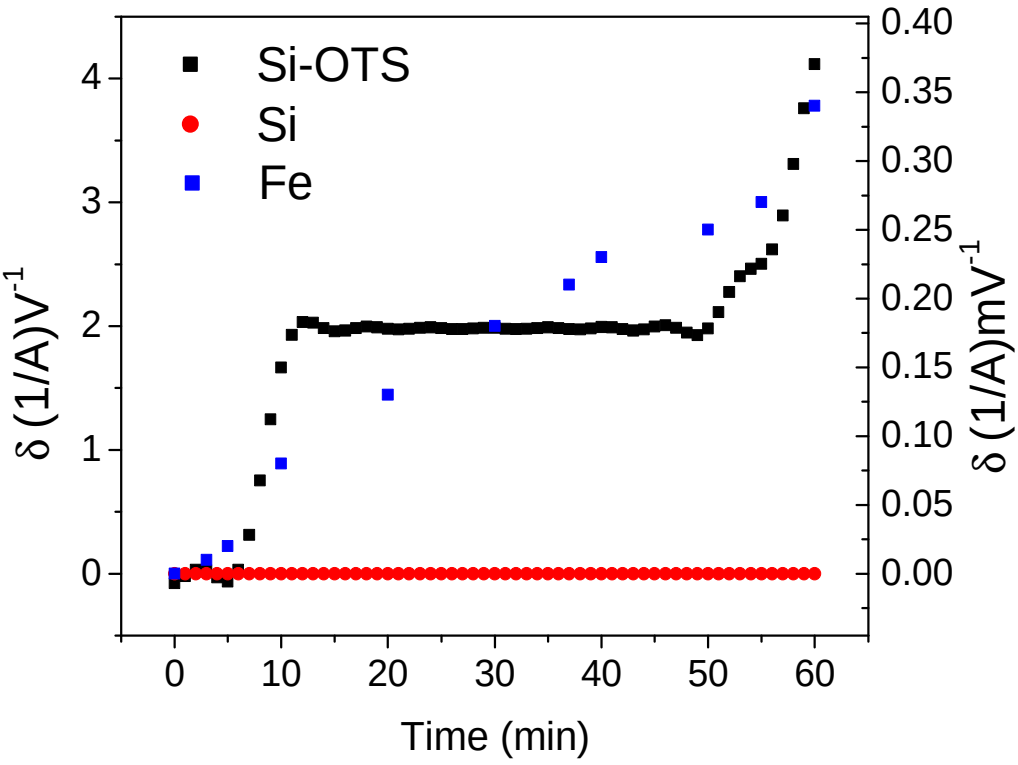

Figure 4.4 Shifts in amplitude during the uptake of TBPP on Si-OTS film.

The fact that amplitude shifts are in fact observed indicate that the film is either slipping on account of the oscillatory motion of the microbalance, or else exhibiting an internal molecular motion within the TBPP molecules themselves. The uptake of TBPP on Si surface alone did not exhibit any amplitude shifts, indicating a solid film adsorbed on the surface with no slippage.

These results indicate that TBPP is a possible candidate for lubricating the MEMS devices, especially those released using self-assembled monolayers like OTS.

CHAPTER 5

EXPERIMENTAL APPARATUS AND PROCEDURE:

MEMS FRICTION TESTERS

5.1 Introduction

In this chapter, I will explain the test structures used, their operation, the circuitry designed to drive them, and the experimental apparatus and procedures used to study the friction of these microstructures.

5.2 Study of uptake of VPL on Test structures

The test structures, surface micromachined Sidewall tribometers (Friction testers), were specially designed by Sandia National Laboratories to determine the friction co-efficient of the micromachined structures. Five dies, each having four friction testers were obtained. The devices were not released when they were received from Sandia Labs. These sidewall tribometers were fabricated using SUMMiT Technology process. They were then sent for release at MCNC. Care was taken to dry the released samples using supercritical CO_2 technique, in order to avoid stiction at the release stage.

Each die was then wire-bonded in a 64-pin DIP package. One of the samples was wire-bonded using a Gold ball bonder. The remaining dies were wire-bonded

using Aluminum manual wedge bonder. The Figure 5.1 illustrates the wire bonding in a 64-pin package.

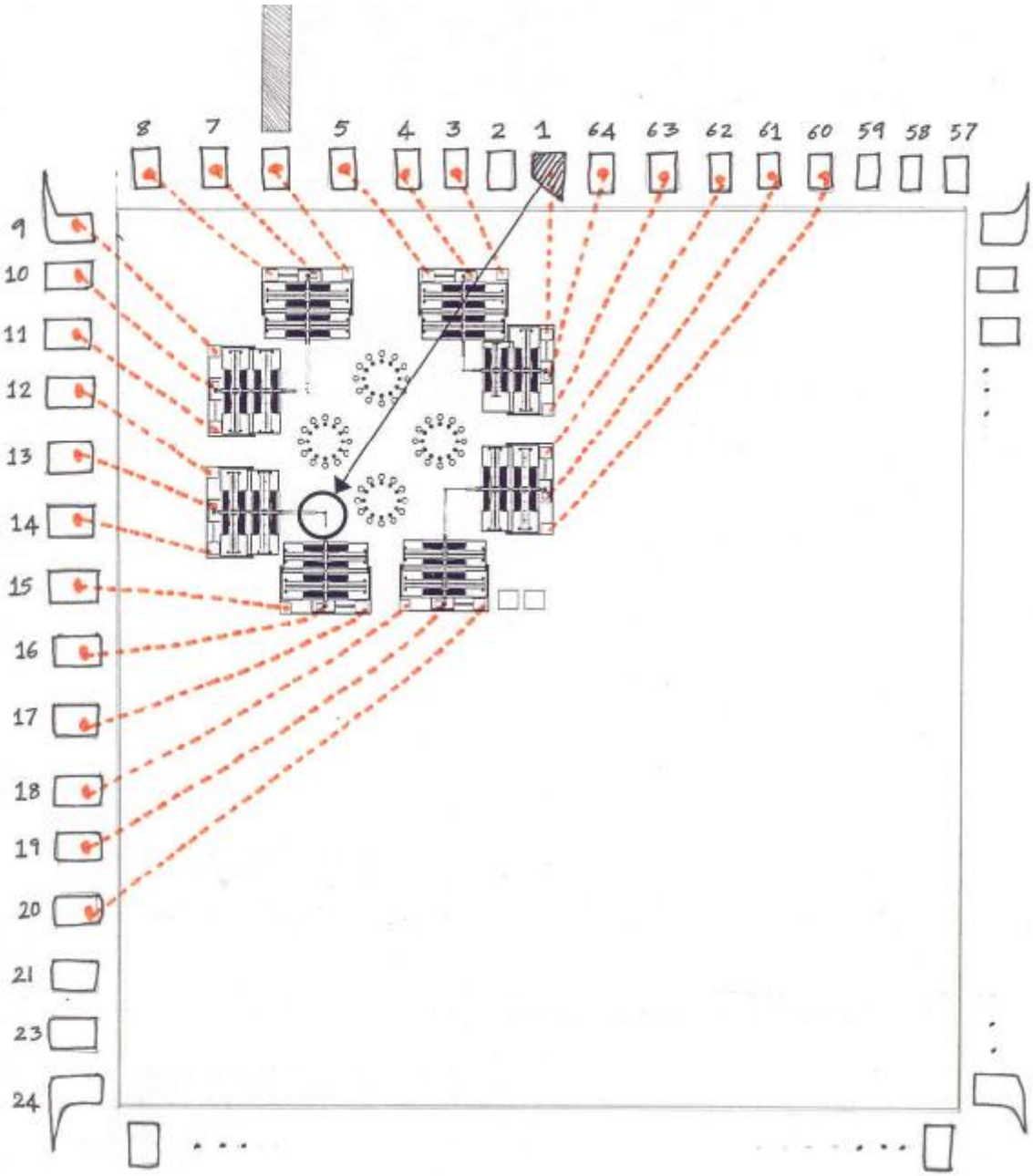

Figure 5.1 Wire-bonding diagram

5.2.1 Surface micro-machined Sidewall tribometer (Friction Tester)

Friction testers from Sandia National Labs are specially designed tribology test structures used to determine the friction between micromachine structural elements. The devices are designed to produce sliding contact between two etched surfaces (sidewalls that are perpendicular to the wafer. A schematic of the test structure is shown in the figure below.

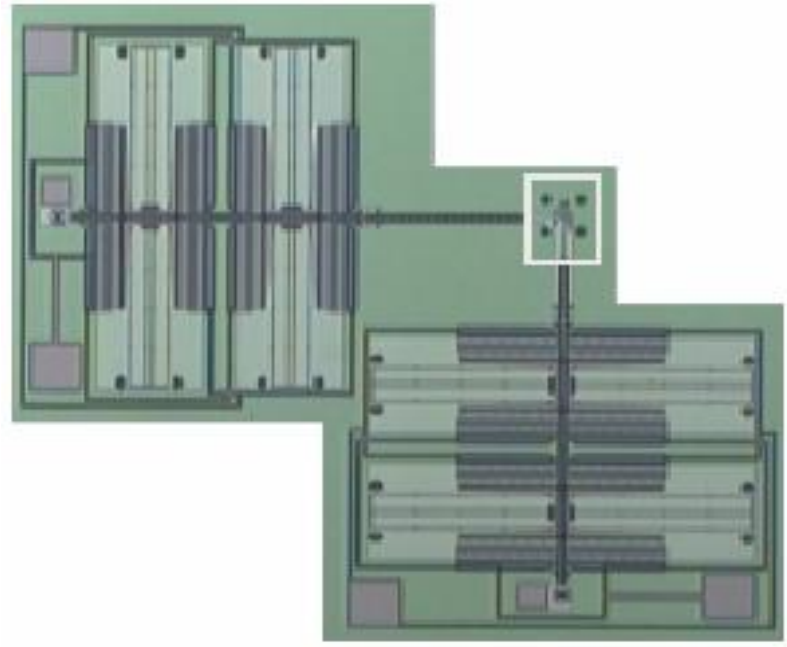

Figure 5.2. Overall view of the sidewall friction tester [44].

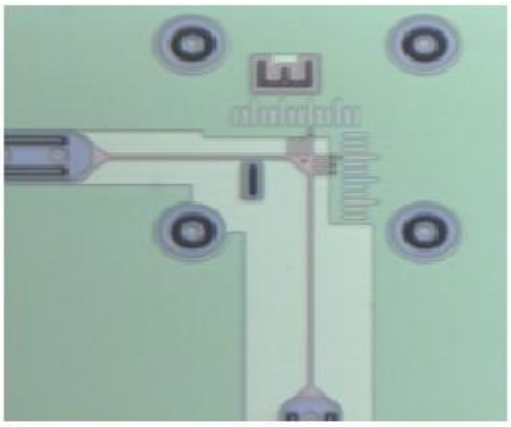

Figure 5.3. Close-up image of the boxed area in fig 3.2

The device is driven using two electrostatic comb-drives. One is used to pull a suspended beam into contact with a fixed semi-cylindrical post, and the other is used to oscillate the beam against the post under a load. The following figure briefly illustrates the orientation of the two comb-drives with respect to each other.

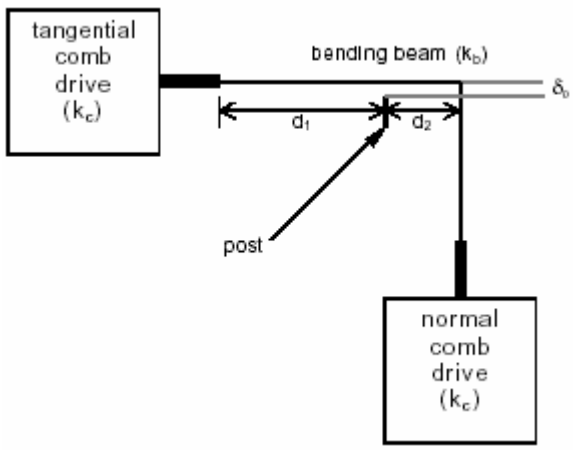

Figure 5.4. Orientation of the two electrostatic comb drives [45]

The polycrystalline silicon post is about 6μm high, which is deposited close to the suspended beam by low-pressure chemical vapor deposition of silicon in a deeply etched trench. The radius of curvature of the post is 2μm. Figure 5.5 gives a closer view of the beam and the post where the contact is made.

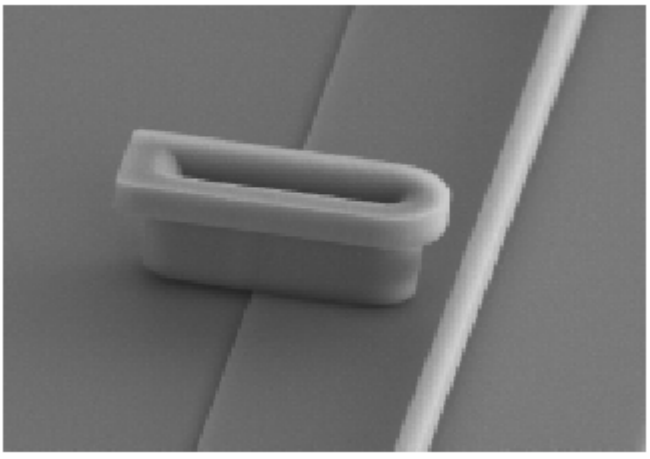

Figure 5.5 Closer view of the area where contact is made [46]

The normal comb drive (N drive), which acts perpendicular to the axis of the flexible polycrystalline silicon beam, loads the beam in contact with the post. This normal load is determined from the deflection of the comb as a function of voltage, the electrostatic force constant, and the spring constants of the comb suspension. The beam is then oscillated with respect to the fixed post using the tangential comb-drive (T drive), which acts parallel to the axis of the beam.

The friction force between the post and the beam is determined from the difference in displacement, when the test device is in contact and out of contact with the fixed post. The electrostatic force produced by the comb-drive is given by,

$$F_C = ½.\ (N\ t\ e_O\ e_r\ V^2)/g \qquad (1)$$

where V is the applied electric potential, N is the number of fingers, ε_O is the permittivity in free space, ε_r is the relative permittivity of the dielectric material between the two electrodes (fingers), t is the thickness of the finger, and g is the gap between the two fingers.

Under equilibrium conditions, the electrostatic force is equal to the restoration force associated with the stiffness of the comb-drive system due to its displacement, giving

$$F_C = ½.\ (N\ t\ e_O\ e_r\ V^2)/g = (k_c + k_b).\ \delta_o \qquad (2)$$

where k_c is the stiffness of the comb suspension springs, k_b is the stiffness of the beam in bending and δ_0 is the displacement of the comb-drive. When the comb-drive is in motion, in the absence of contact, the force balance yields,

$$F_C - (k_c + k_b)\ x_o = m.\ d^2x_o/dt^2 \qquad (3)$$

where x_0 is the displacement of the comb-drive at any point in time in the absence of the load. When the suspended beam is pulled in contact with the post, a frictional drag force f_d is created, and the force balance becomes,

$$F_C - (k_c + k_b)\, x - f_d = m.\, d^2x/dt^2 \qquad (4)$$

where x is the displacement of the comb-drive at any point in time in the presence of contact. As the system reaches equilibrium,

$$d^2x/dt^2 \rightarrow 0$$
$$x_o \rightarrow \delta_o \text{ and } x \rightarrow \delta$$

where δ and δ_0 are the equilibrium displacements with and without friction respectively. Since the electrostatic force in the comb drive is the same in both the cases, equations (3) and (4) may be expressed in terms of F_C, equated and solved for f_d, yielding,

$$f_d = (k_c + k_b)\,(\delta_o - \delta) \qquad (5)$$

Substituting for $(k_c + k_b)$ from equation (2),

$$f_d = (F_C / \delta_o).\,(\delta_o - \delta) \qquad (6)$$

$$= F_C\,(1 - \delta/\delta_o) \qquad (7)$$

The friction co-efficient is then obtained by dividing the frictional force by the applied normal load (electrostatic force associated with the normal comb-drive).

Each friction test structure, which includes the tangential comb-drive and the normal-comb drive, requires five signal lines to operate. Two of the drive signals are the oscillating voltages, 180° out of phase, with $V_{p\text{-}p} \approx$ 50V – 60V, and oscillating frequency of 100Hz. These signals are used to drive the tangential comb-drive, which oscillates the beam against the fixed post driven by a square wave output (100Hz). The other two drive signals are push/pull DC voltages with amplitude ±40V. These drive signals are used to pull the suspended beam in contact with the post. The fifth signal line is the reference/ ground line.

Several techniques have been devised to determine to amplitude of the beam position at the beam/post interface. Dugger *et al* used image-processing techniques to determine the distance moved by the beam, by determining the position of the 'dot' at the end of the beam. Subtracting coordinates from images representing the limits of motion of the device enabled the displacement amplitude to be determined. While the beam is at each limit of motion, a strobe is triggered and an image of the beam and post is acquired with a CCD camera and a frame grabber [47].

In this study, we quantify the amplitude of the beam position at the beam/post interface using a novel optical technique. A laser beam is made to focus on the test structure, the reflected beam is then sensed by a photo-detector circuit, which converts the light intensity into a corresponding voltage. The amount of light falling on the photo-diode depends on the amplitude of motion of the friction-tester [To be published later]. Several samples of the output voltages, with the beam not in contact are acquired to determine the amplitude of the beam motion without friction at the beam/post interface. A DC voltage is then applied to bring the beam in contact with the post. The output voltages are recorded as the device is run for several cycles after loading. Once the displacement of the beam is obtained, the friction co-efficient is calculated as shown above.

5.2.2 Comb drive theory

Comb drives consist of a set of fixed electrodes (or fingers) and a set of movable electrodes (or fingers) placed interdigitated with each other. The driving principle of the electrostatic Comb-Drive actuator is based on electrostatics [48]. Figure 3.6 illustrates a Comb-Drive actuator.

When voltage is applied to the movable electrodes while the fixed electrodes are potentially grounded, a potential difference develops across the fingers and they become electrically charged. This action induces a capacitance in the charged electrodes. This results in an electrostatic force being generated, causing a displacement in the x direction. The force F created in the comb is given by,

$$F = \tfrac{1}{2}.\ (N\ t\ \varepsilon_O\ \varepsilon_r\ V^2)/g$$

where V is the applied electric potential, ε_r is the relative permittivity of the dielectric material between the two electrodes, ε_O is the permittivity in the free space equal to 8.85pF/m, n is the number of pairs of electrodes (fingers), t is the thickness of the finger, and g is the gap between the two fingers.

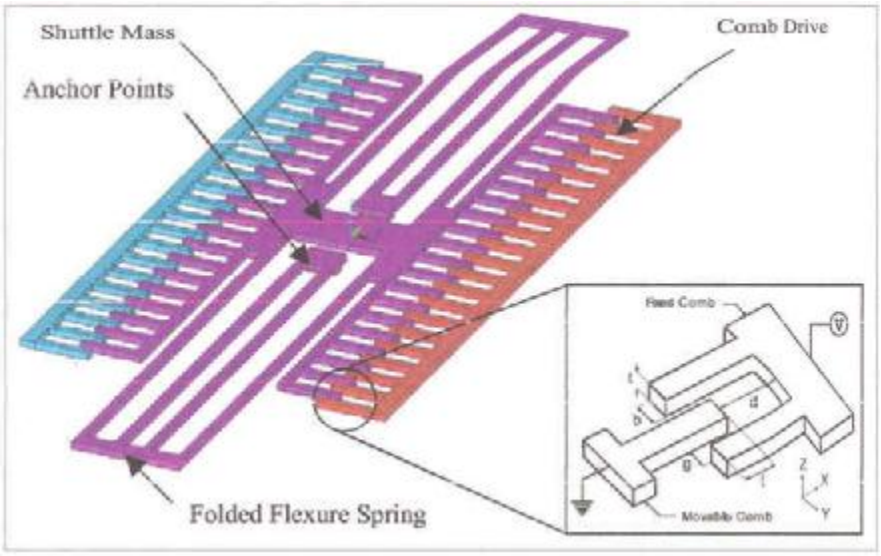

Figure 5.6. Comb-Drive. [48]

A reaction force F_S is induced in the suspension beam holding the movable set of fingers. This suspension beam, which represents a spring suspension system, is related to the stiffness of the beam and the displacement. The relationship is given by the following equation,

$$F_S = K_X.\ x$$

where, K_X is the spring stiffness in the direction of actuation, and x is the displacement. If the beam stiffness is higher, a larger electrostatic force is required to cause the deflection, which means a higher driving voltage is required. In the equilibrium position, the forces F and F_S are equal.

5.2.3 Comb-drive preliminary test

The comb-drives were initially tested to ensure proper release. A simple electrically induced deflection test was used to determine if the resonant structure could be electrically operated. A DC bias was applied to one of the fixed comb finger electrodes while the other fixed electrode and the suspended structure (shuttle mass) are electrically grounded. The DC bias was gradually increased to observe the displacement of the suspended structure. This test provided a good estimate of the magnitude of bias required to achieve a desired displacement of the structure.

5.2.4 Electronic circuitry to drive the MEMS devices

The friction testers used in this study require fairly high input voltages to drive them. As mentioned in the previous section, each friction tester consists of a tangential comb drive and a normal comb drive. The normal comb drive requires DC voltages greater than ± 40V to bring the suspended beam in contact with the post. The tangential comb drive requires two square wave signals, 180° out of phase with $V_{p\text{-}p}$ greater than ± 40V to oscillate the beam against the post.

The DC voltage is obtained by converting the wall voltage (AC) to a corresponding high DC voltage, using an *Acopian* unregulated power supply. The square wave oscillating signals, 180° out of phase with each other, are obtained using a high voltage operational amplifier circuit. Figure 5.7 is a block diagram of the electronics required.

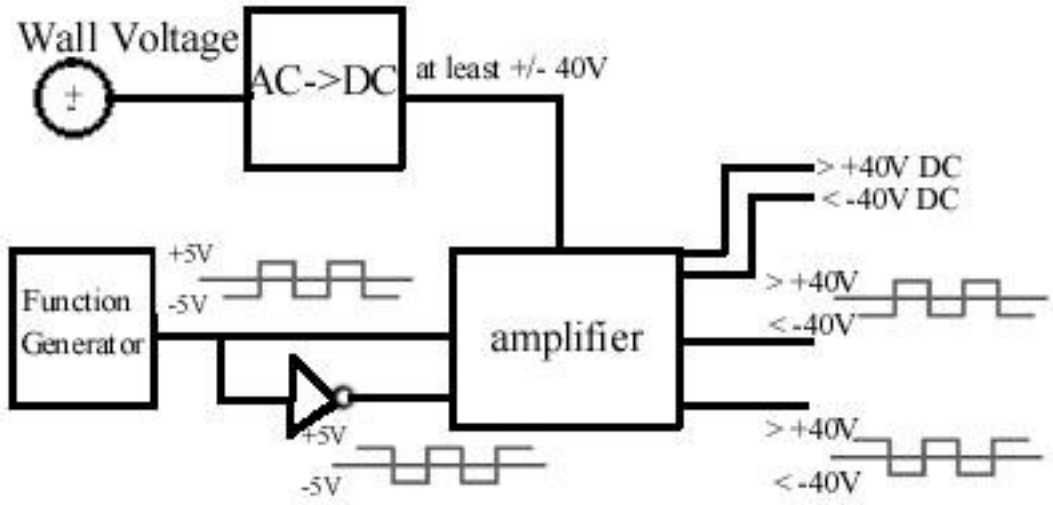

Figure 5.7 Block diagram of the electronic drive circuitry [49]

5.2.5 High-voltage operational-amplifier circuit

The high-voltage op-amp amplifier circuit was designed to obtain the push/pull oscillating drive voltages with peak amplitudes as high as 70V p-p, 180 degrees out of phase, to run the comb drives of the friction testers. The ideal operating frequency of these comb drives is 100Hz, but the amplifier is designed to give the required amplification at a range of frequencies. Op-amps were chosen for their high gain and stability due to heavy feedback. Also, these op-amps can be replaced without affecting the circuit gain.

The amplifier circuit employs two PA88 high-voltage power operational amplifiers manufactured by Apex Microtechnology. The PA88 is a high voltage, low quiescent current MOSFET operational amplifier designed for output currents up to 100mA. Output voltages can swing up to +/- 215V with a dual supply and up to +440V with a single supply. The push/pull oscillating voltages which are 180 degrees out of phase are obtained by designing the circuit in inverting and non-inverting configuration respectively. The following figure gives the design of the high-voltage op-amp circuit.

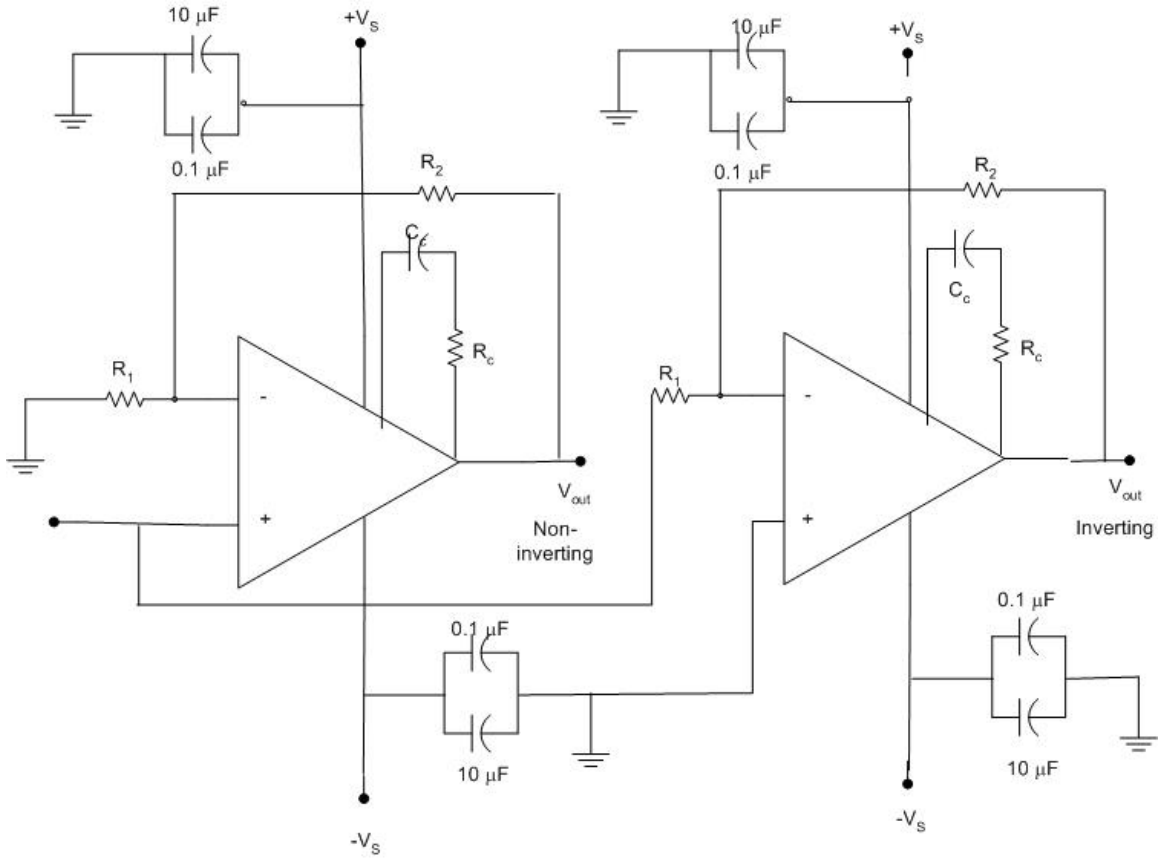

Figure 5.8. Schematic of the high-voltage operational amplifier circuit.

The gain of the inverting configuration G_{inv} is calculated as $-R_2/R_1$. The closed loop gain G_{in} is defined as

$$G_{inv} \ @ \ V_{O(inv)}/V_{in}$$

If V_1 and V_2 are voltages at the inverting and non-inverting terminals respectively, V_1 approaches V_2 because of the infinite gain A of the operational amplifier. By definition,

$$V_2 - V_1 = V_{O(inv)} / A \approx 0$$

Since the inverting configuration has the non-inverting terminal connected to ground, the current i_1 through the resistor R_1 follows,

$$i_1 = (V_{in} - V_1)/ R_1 \approx V_{in}/R_1$$

Applying Ohm's law,

$$V_{O\,(inv)} = V_1 - i_1 R_2$$
$$= 0 - V_{in}/R_1 . R_2$$

Thus,

$$V_{O(inv)}/ V_{in} = -R_2/R_1$$

In the non-inverting configuration, V_{in} is applied to the non-inverting terminal. The output voltage is given by,

$$V_{O\,(non\text{-}inv)} = V_1 + (V_1/R_1)\, R_2$$

which yields,

$$V_{O\,(non\text{-}inv)}/ V_{in} = 1 + (R_2/R_1)$$

The PA88 has sufficient phase margin to be stable with most capacitive loads, using the recommended phase compensation. The phase compensation network R_C and C_C are chosen to be 100Ω and 33pf respectively, for this application. Figure 5.9 shows the external connections of the PA88.

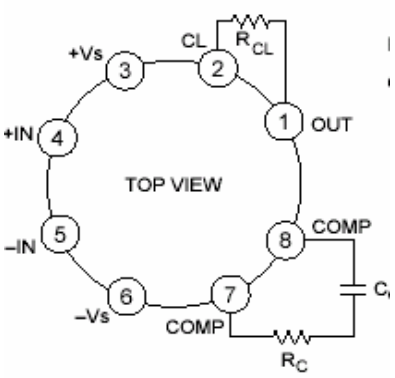

Figure 5.9 Top view and pin configuration of PA88 [50]

The equivalent schematic of the PA88 is as shown below.

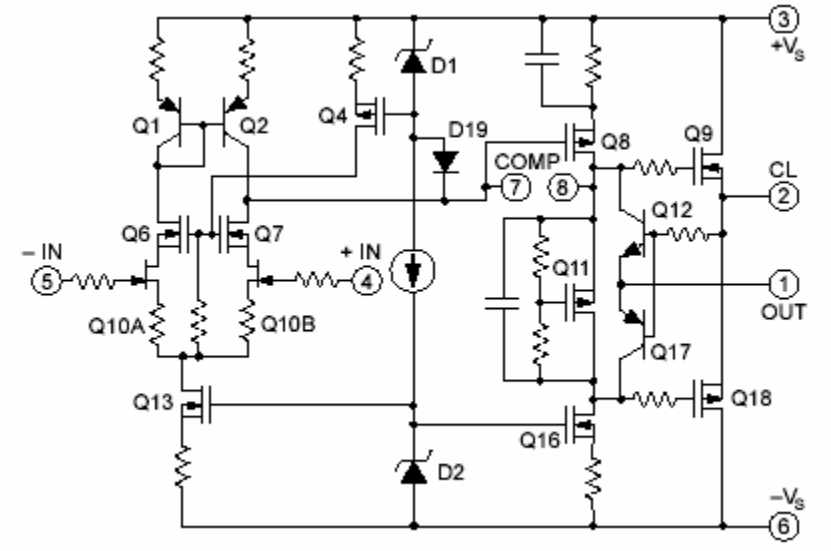

Figure 5.10 Schematic of the PA88 [50]

5.2.6 Power supply

A dual output AC – DC power supply by *Acopian* was used to convert the wall voltage to the required high-voltage power supply to the PA88 operational amplifiers.

5.2.7 Camera trigger and Image capture

A *PanasonicGP-MF622* CCD camera was used to capture images of the test structures in this study. Designed to withstand strong vibration, its high speed electronic shutter is ideal to capture the suspended beam in motion. A high speed flash would not have worked, since reflection and refraction problems would be more prominent through the vacuum view port.

The output of the camera is sent to a frame grabber, which can be electronically triggered. The camera can thus freeze the video through a trigger signal, and the frame grabber is used to store the image on a hard drive. *Flash Point 3D* frame grabber was used here in this study.

The following shows the DIP switch configuration that will set the camera to external triggering, with a shutter speed of 1/8000 sec [49].

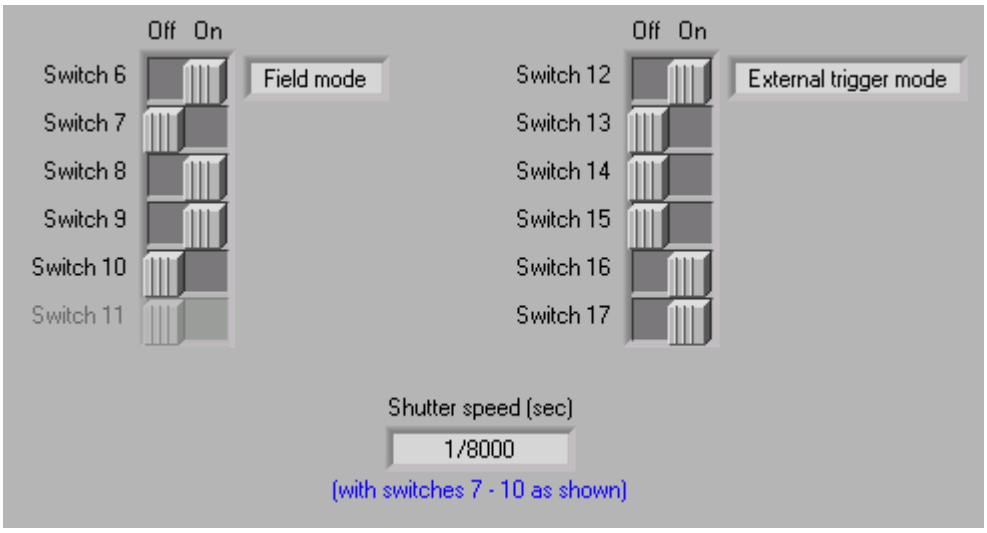

Figure 5.11. DIP switch configuration for the CCD camera. [49]

5.2.8 Ultra High Vacuum (UHV) setup description

The test structures were housed in the Ultra High Vacuum system while conducting the experiments. The UHV setup was built for ultra high vacuum

compatible materials. However, the experiments were conducted in the range of 1.0 X 10^{-7} to 1.0 X 10^{-8} Torr, since the application did not require a ultra high vacuum environment. One of the main problems encountered during this study was the problem associated with vibration. Vibration isolation was achieved by suspending the entire UHV system using bungee chords, which were hung from a steel support structure. This simple, yet effective solution helped a great deal to eliminate the vibrations. Figure 5.12 shows the photograph of the UHV setup.

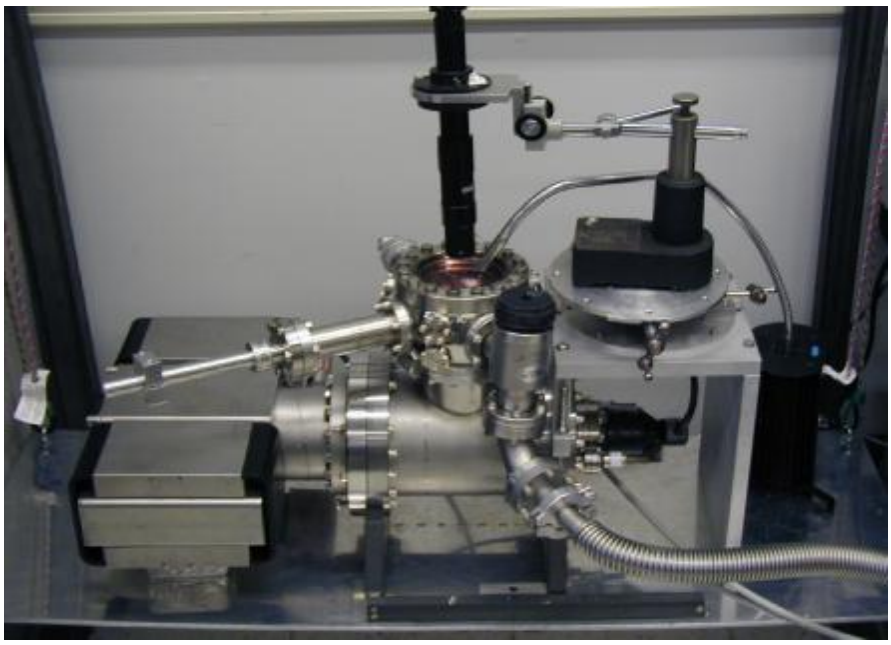

Figure 5.12.Photograph of the UHV setup.

The base pressure in the vacuum system was maintained at 1.0 X 10^{-7} Torr. The UHV chamber basically consists of a T shaped stainless steel chamber, the horizontal chamber is the main chamber, whereas the vertical chamber is the experimental chamber, to which are attached the sample holder, electrical feedthrough, lubricant reservoir, laser beam positioner, photodetector, and the turbo and diaphragm pumps. The pressure gauge and the Ion pump are attached to the main chamber.

The Panasonic CCD camera is positioned over the vacuum viewport of the experimental chamber, to facilitate image capturing of the test structures. Fiber-Lite fiber optic illuminators were used over the vacuum viewport to provide the lighting to view the devices through the camera. The following figure illustrates the same.

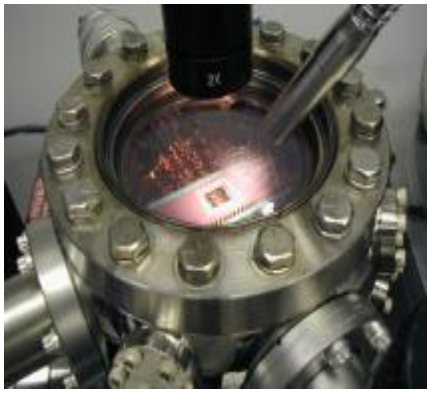

Figure 5.13. Photograph of the vacuum viewport.

A valve ‘V1’ separates the experimental chamber and the turbo and ion pumps. Open to the experimental chamber with another valve ‘V2’ is the lubricant reservoir, which is always kept closed except while conducting the experiments. The turbo and diaphragm pumps, are used to pump down the system starting from atmospheric pressure, 760 Torr, to 10-5 Torr range. After this stage, the ion pump took over. Figure 5.14 illustrates the experimental setup schematic that has been put together and employed to conduct the study.

The whole system was typically baked at about 100°C for a period of 24 to 48 hours. By employing the turbo and diaphragm pumps, and the ion pump in the later stages, the system routinely reaches the low base pressure of 1.0 X 10-7 Torr.

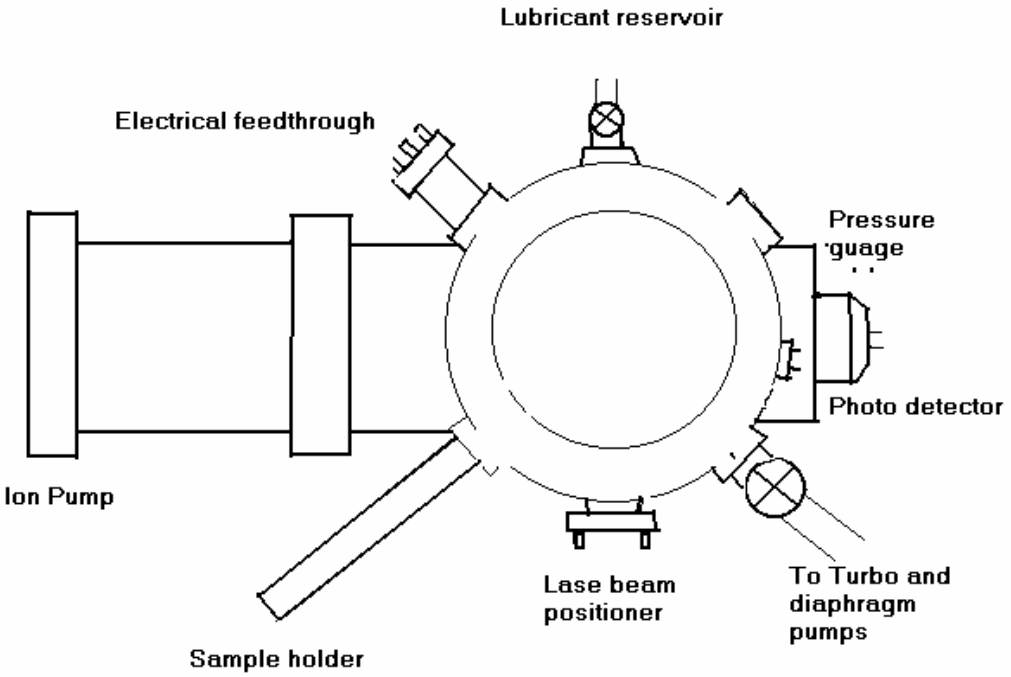

Figure 5.14. Schematic of the UHV setup.

CHAPTER 6

MEMS FRICTION TESTERS

6.1 Introduction

This chapter shows the work done until now with respect to the MEMS friction testers. The biggest challenge was to get the comb-drives oscillating and find a method to quantify the amplitude of motion. Considerable time was spent to identify the working comb-drives since many of these devices were destroyed during the release stage due to stiction. A novel method to detect the motion of these microstructures was devised, using laser-photodetector set-up.

6.2 Set-up to detect the motion of the test structures

Determining the amplitude of motion of these test structures is very important in this study, since the friction co-efficient is deducted from these measurements. So far, optical camera/ frame grabbing methods have been used to determine the amplitude of motion. A novel laser-photodetector technique, which exhibits considerable precision is used to determine the motion of these microstructures. Figure 6.1 shows the photograph of the set-up used.

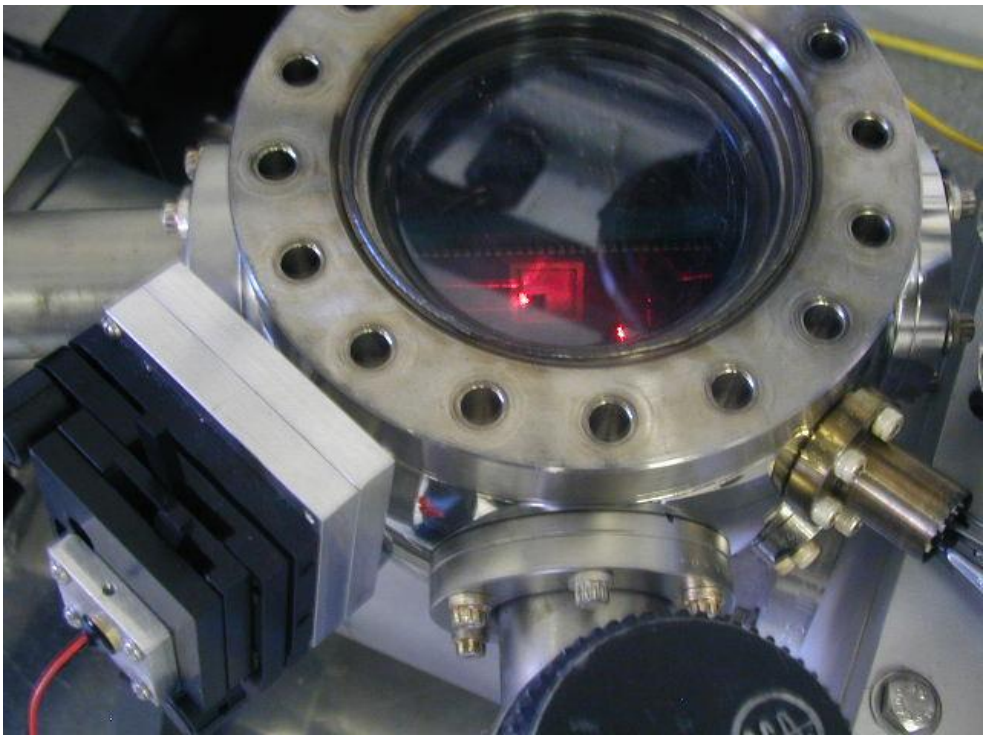

Figure 6.1 Photograph of the Laser-Photodetector setup.

A thin laser-beam is made to focus on the desired test-structure whose amplitude of motion is to be determined. The reflected light is then captured by a photodiode, the output of which is connected to a trans-resistance photodetector circuit, which converts the photodiode current to a voltage level.

The output of the photodetector circuit was captured by Flukemeter. The following result shows the response of the photodetector circuit to motion of the friction testers, driven by 60 V drive voltage.

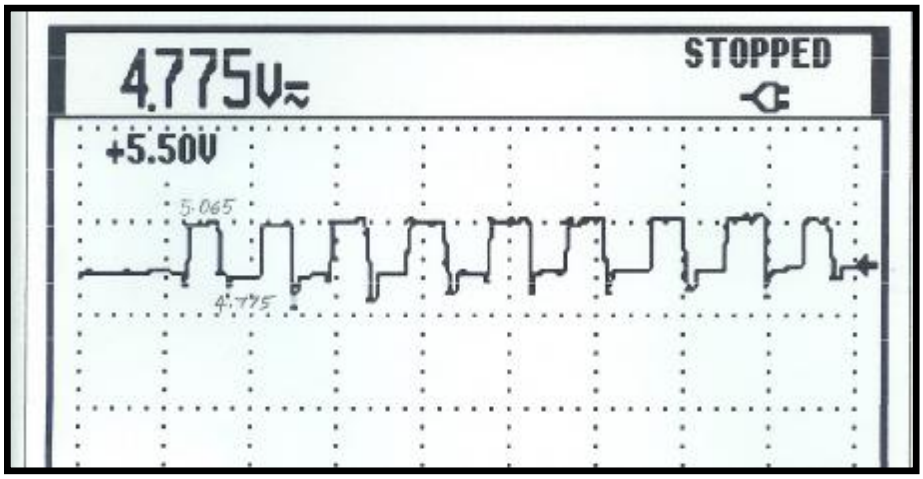

Figure 6.2 Response of the photo-detector circuit to the motion of the friction testers.

The above mentioned set-up was found to have a good precision , and a vast improvement to the optical/ camera frame grabbing techniques which involve image processing techniques. The relationship between the output voltage of the trans-resistance photodetector circuit and the amplitude of motion of the comb-drives is being determined. The details of the Laser photodetector sensor of MEMS friction tester motion will be provided in a later publication.

CHAPTER 7

CONCLUSIONS

At room temperature, Si was found to adsorb the vapor phase lubricant t-butyl phenyl phosphate (TBPP), though the lubricant did not show any slippage. On the other hand the adsorption of TBPP on Si coated with OTS did show some slippage, though it has a relatively much less adsorption. These results indicate that TBPP is lubricating the Si-OTS surface. The SAM coating of OTS is known to degrade at higher temperatures. Since TBPP has high temperature stability, we can conclude that this vapor phase lubricant would in fact protect the OTS coating at high temperatures. The vapor phase lubricant TBPP and the SAM coating OTS seem to exhibit a synergistic relationship. The experiments conducted with the silver electrode quartz crystals placed at various positions within the experimental vacuum chamber indicate that the lubricant is conformal.

We have managed to build a system for the uptake of vapor phase lubricants on the MEMS friction testers under vacuum conditions. This new and improved friction test setup will help in understanding the frictional characteristics of these microstructures, and possibly aid in developing a reliable solution to overcome the myriad problems associated with friction and stiction of MicroElectro Mechanical Systems. A laser sensor system has been devised to quantify the amplitude of motion

of these microstructures, which is a vast improvement over the conventional frame grabbing and image processing technique.

Summarizing the accomplishments during the various stages of this thesis,

- Built the ultra high vacuum chamber for the Quartz crystal microbalance experiment, to study the uptake of the vapor phase lubricant on Si and Si-OTS surfaces.
- Studied the behavior of t-butyl phenyl phosphate uptake on Si and Si-OTS surface.
- Built the ultra high vacuum chamber for the MEMS friction testers, to facilitate the screening of vapor phase lubricants under a controlled environment.
- Got the MEMS test structures released and wire-bonded the die containing these test structures onto a 64-pin package.
- Developed the laser-photodiode sensor for the MEMS friction testers.
- Designed the electronic circuitry to generate the required drive signals for the MEMS structures.

Future work will be performed, using existing system capabilities to study the change in friction co-efficient after screening of the vapor phase lubricant TBPP. Further work involves the study of various other vapor phase lubricants using the QCM set-up and screening these lubricants onto the MEMS friction testers to compare the friction characteristics.

BIBLIOGRAPHY

[1] All About MEMS, a website for full range information about MicroElectro Mechanical Systems.[http://www.allaboutmems.com/memsapplications.html]

[2] N. Maluf, "*An Introduction to Microelectromechanical Systems Engineering*," Artech House, Boston: 2000.

[3] "*Surface Micromachining: A Brief Introduction"* Mehran Mehregany and Christian Zorman.

[4] R. L. Alley, P. Mai and R. T. Howe, "*Surface roughness modification of interfacial contacts in polysilicon microstructures*," in Proc.7th Int. Conf. Solid-State Sensors and Actuators-Transducers'93, Yokohama, Japan, pp. 288-292.

[5] T. Abe, W. C. Messner, and M. L. Reed, "*Effects of elevated temperature treatments in microstructure release procedures*," IEEE J.MEMS, vol4, pp. 66-75, 1995.

[6] G. T. Mulhern, D. S. Soane, and R. T. Howe, "*Supercritical carbon dioxide drying of microstructures*," in Proc. 7th Int. Conf. Solid-State Sensors and Actuators- Transducers'93, Yokohama, Japan, pp. 296-300.

[7] S. L. Miller, J. J. Sniegowski, G. LaVigne, and P. J. McWhorter, "*Friction in surface micromachined microengines*".

[8] R. L. Aleey, P. Mai, K. Komvopoulos, and R. T. Howe, "*Surface Roughness modification of Interfacial Contacts in Polysilicon Microstructures*," Intl. Conf. Solid-State Sensors and Actuators, Yokohama, Japan, 1993, pp.288-291.

[9] B. Bhushan ed., Tribology Issues and Opportunities in MEMS (Kluwer Academic Publishers, Boston, 1998).

[10] M. R. Houston, R. T. Howe, and R. Maboudian, "*Effect of hydrogen termination on the work of adhesion between rough polycrystalline silicon surfaces*," J. Appl. Physics., vol.81.

[11] U. Srinivasan, M. R. Houston, R. T. Howe, "*Alkyltrichlorosilane-Based Self Assembled Monolayer Films for stiction reduction in silicon micromachines*". J.MEMS.,vol 7.

[12] http://www.chem.qmw.ac.uk/surfaces/scc/scat4_2.htm

[13] Andrew J. Gellman and Jeff S. Ko, "*The current status of tribological surface science*", Tribology Letters Vol. 10, No. 1-2, 2001.

[14] http://www.chem.qmw.ac.uk/surfaces/scc/scat4_1.htm

[15] http://www.virtis.com/pages/freez.html

[16] C. H. Mastrangelo,"*Adhesion related failure mechanisms in micromechanical systems*", Tribology letters.

[17] N. Takeshima, K. J. Gabriel, M. Ozaki, J. Takashashi, H. Horiguchi, and H. Fujita, "*Electrostatic parallelogram actuators*," in *Transducers' 91*, pp. 63–66, 991.

[18] Lee Y-I, Park K-H, Lee J, Lee C-S, Yoo H-J, Kim C J and Yoon Y-S 1997," *Dry release for surface micromachining with HF vapor-phase etching*", *J. MEMS* 6 226–33

[19] Xuan-Qi Wang, Xing Yang, and Yu-Chong Tai," *Gas-Phase Silicon Etching with Bromine Trifluoride*," Technical Digest, 1997 International Conference on Solid-State Sensors and Actuators (Transducers '97), Chicago, IL, Jun. 16-19 (1997).

[20] Liu, C., T. Tsao, and Y. C. Tai, "*A High-Yield Drying Process for Surface-Micromachined Structures Using Magnetostatic Forces*," Journal of Sensors and Materials, 11:2, 71-86, 1999.

[21] D. Kobayashi, C.-J. Kim, and H. Fujita, "*Photoresist-Assisted Release of Movable Microstructures.*" Japanese J. Applied Physics, Vol 32, No. 11A, 1993, pp. L1642-L1644.

[22] T. Abe, W. C. Messner, and M. Reed, "*Effective methods to prevent stiction during post-release-etch processing,*" Proc. IEEE Micro Electro Mech. Syst. Workshop,Amsterdam, Neth, Feb. 1995, pp. 94–99.

[23] B. P. Gogoi and C. H. Mastrangelo, "*Adhesion release and yield enhancement of microstructures using pulsed lorentz forces,*" Journal of Microelectromechanical Systems, vol. 4, pp. 185–192, 1995.

[24] Smella et al., "*Differential adhesion method for microstructure release: An alternative to the sacrificial layer*".

[25] Brian D. Knutson, "*The Use of Supercritical Carbon Dioxide-Based Solvents as*

a Cost Effective and Environmentally Sound Alternative to Current Photoresist Stripping Solvents".

[26] L. B. Rothman, R. J. Robey, M. K. Ali, "*Supercritical fluid processes for semiconductor device fabrication*".

[27] E. M. Russick, C. J. Adkins, C. W. Dyck., "Supercritical *carbon dioxide xtraction of solvent from micromachined structures*".

[28] R. Maboudian, W. R. Ashurst, C. Carraro,. "*Self Assembled Monolayers as Anti-stiction coatings for MEMS: Characteristics and recent developments*".

[29] U. Srinivasan, M. R. Houston, R. T. Howe, and R. Maboudian, "*Self-assembled fluorocarbon films for enhanced stiction reduction,*" in Transducers' 97, pp. 1399–1402, 1997.

[30] Y. Yee, K. Chun, and J. D. Lee, "*Polysilicon surface modification technique to reduce sticking of microstructures,*" in Transducers' 95, pp. 206–209, 1995.

[31] S. S. Mani, J. G. Fleming, J. A. Walraven, J. J. Sniegowski, M.P. de Boer , L.W. Irwin, D.M. Tanner, D.A. LaVan, J. Jakubczak, and W.M. Miller, "*Effect of W coating on microengine performance*"—Sandia National Laboratories, Albuquerque, NM.

[32] F. Kozlowski, N. Lindmair, T. Scheiter, C. Hierold, andW. Lang, "*A novel method to avoid sticking of surface micromachined structures," Transducers'95,* pp. 220–223, 1995.

[33] M.R. Houston, R. Maboudian, and R.T. Howe , "*Ammonium Fluoride Anti-Stiction Treatments for Poly-Silicon Microstructures*", *Proceedings of the 8th International* Conference on Solid-State Sensors and Actuators, pp. 210-213 (1995).

[34] W. R. Ashurst, C. Yau, C. Carraro and R. T. Howe, "Alkene Based Monolayer Films as Anti-Stiction Coatings for Polysilicon MEMS", *Proceedings of Solid-State Sensor and Actuator Workshop, Hilton Head 2000,* Hilton Head Island, SC, June 2000, pp. 320-323.

[35] Piu Francis Man, Bishnu P. Gogoi, and Carlos H. Mastrangelo, " *Elimination of Post-Release Adhesion in microstructures using conformal fluorocarbon coatings*", Journal of MicroElectro Mechanical Systems, Vol 6, No 1, March 1997.

[36] U. Srinivasan, M. R. Houston, R. T. Howe, and R. Maboudian, "Selfassembled fluorocarbon films for enhanced stiction reduction," in *Proc.9th Int. Conf. Solid-State Sensors and Actuators—Transducers'97*,Chicago, IL, pp. 1399–1402.

[37] *Thin Teflon-Like Films for Eliminating Adhesion in Released Polysilicon Microstructures,* B. K. Smith, J. J. Sniegowski, and G. J. LaVigne, (Invited paper) 1997 International Conference on Solid-State Sensors and Actuators, Chicago, IL, June 16-19, 1997, Vol. 1, pp. 245-248.

[38] D. Salt, Hy-Q "*Handbook of Quartz crystal devices*" Van Nostrand Reinhol (UK), T. J.Press, Cornwall.

[39] PVD Deposition Monitors : QCM by Seann Bishop, NC State University.

[40] L. Brushi et al, "*Inexpensive but accurate driving circuits for QCMs*"., Review of Scientific Instruments, vol 70.

[41] Thesis dissertation: "*Nanotribology of Vapor phase lubricant, Quartz crystal microbalance study of tricresylphosphate (TCP) uptake on Iron and Chrome*"., by Mohamed Abdelmaksoud.

[42] J. Krim and Widom, Phy.Rev. B38, 12184,1988;A. Widom and J. Krim, Phy.Rev. B34, 1986.

[43] B. L. Mason, S. M. Winder and J. Krim, "*On the current status of quartz crystal microbalance studies of superconductivity-dependent sliding friction*"., Tribology Letters, 2001.

[44] W. Robert Ashurst, Christina Yau, Carlo Carraro, Christina Lee, G. Jonathan Kluth, Roger T.Howe*, and Roya Maboudian, "Alkene Based Monolayer Films as Anti-Stiction Coatings for Polysilicon MEMS".

[45] W. R. Ashurst, R. Maboudian, C. Yau and C. Carraro, "Dichlorodimethylsilane as an Anti-Stiction Coating for MEMS".

[46] M. T. Dugger, D. C. Senft and G. C. Nelson., "*Friction and durability of chemisorbed organic lubricants for MEMS*"., Sandia National Laboratories.

[47] M. T. Dugger., "*Quantification of friction in microsystem contacts*"

[48] W. A. Mousssa, H. Ahmed, W. Badawy, M. Mousssa., "*Ivestigating the reliability of electrostatic comb-drive actuators utilized in microfluidic and space systems using finite element analysis"*.

[49] Christina Hammock, Chloe Palenchar, Danny Wise, “MEMS tech”, Final report on MEMS.

[50] PA88 Data sheet, Apex Microtechnology.

[51] D. G. Placek, T. Freiheit, “*Progress in Vapor Phase Lubrication Technology*”., Transactions of the ASME.

[52] B. Borovsky, M. Abdelmaksoud and J. Krim, “STM-QCM studies of vapor phase lubricants”.